Journal of Geophysical Research: Solid Earth

RESEARCH ARTICLE
10.1029/2018JB015706

Special Section:
Magnetism in the Geosciences - Advances and Perspectives

Signatures of Reductive Magnetic Mineral Diagenesis From Unmixing of First-Order Reversal Curves

Andrew P. Roberts[1], Xiang Zhao[1], Richard J. Harrison[2], David Heslop[1], Adrian R. Muxworthy[3], Christopher J. Rowan[4], Juan-Cruz Larrasoaña[5,6], and Fabio Florindo[7]

[1]Research School of Earth Sciences, Australian National University, Canberra, ACT, Australia, [2]Department of Earth Sciences, University of Cambridge, Cambridge, UK, [3]Department of Earth Science and Engineering, Imperial College London, South Kensington Campus, London, UK, [4]Department of Geology, Kent State University, Kent, OH, USA, [5]Instituto Geológico y Minero de España, Unidad de Zaragoza, Zaragoza, Spain, [6]Institute of Earth Sciences Jaume Almera, Consejo Superior de Investigaciones Científicas, Barcelona, Spain, [7]Istituto Nazionale di Geofisica e Vulcanologia, Rome, Italy

Key Points:
- First-order reversal curve unmixing is used to identify characteristic magnetic components and processes in each reductive diagenetic stage
- Detrital/biogenic magnetic minerals dissolve through the ferruginous-sulfidic zones and mainly disappear at the sulfate-methane transition
- Authigenic pyrrhotite and greigite grow in methanic environments with potentially significant paleomagnetic recording delays

Correspondence to:
A. P. Roberts,
andrew.roberts@anu.edu.au

Citation:
Roberts, A. P., Zhao, X., Harrison, R. J., Heslop, D., Muxworthy, A. R., Rowan, C. J., et al. (2018). Signatures of reductive magnetic mineral diagenesis from unmixing of first-order reversal curves. *Journal of Geophysical Research: Solid Earth*, *123*, 4500–4522. https://doi.org/10.1029/2018JB015706

Received 1 MAR 2018
Accepted 15 MAY 2018
Accepted article online 24 MAY 2018
Published online 13 JUN 2018

Abstract Diagenetic alteration of magnetic minerals occurs in all sedimentary environments and tends to be severe in reducing environments. Magnetic minerals provide useful information about sedimentary diagenetic processes, which makes it valuable to use magnetic properties to identify the diagenetic environment in which the magnetic minerals occur and to inform interpretations of paleomagnetic recording or environmental processes. We use a newly developed first-order reversal curve unmixing method on well-studied samples to illustrate how magnetic properties can be used to assess diagenetic processes in reducing sedimentary environments. From our analysis of multiple data sets, consistent magnetic components are identified for each stage of reductive diagenesis. Relatively unaltered detrital and biogenic magnetic mineral assemblages in surficial oxic to manganous diagenetic environments undergo progressive dissolution with burial into ferruginous and sulfidic environments and largely disappear at the sulfate-methane transition. Below the sulfate-methane transition, a weak superparamagnetic to largely noninteracting stable single domain (SD) greigite component is observed in all studied data sets. Moderately interacting stable SD authigenic pyrrhotite and strongly interacting stable SD greigite are observed commonly in methanic environments. Recognition of these characteristic magnetic components enables identification of diagenetic processes and should help to constrain interpretation of magnetic mineral assemblages in future studies. A key question for future studies concerns whether stable SD greigite forms in the sulfidic or methanic zones, where formation in deeper methanic sediments will cause greater delays in paleomagnetic signal recording. Authigenic pyrrhotite forms in methanic environments, so it will usually record a delayed paleomagnetic signal.

1. Introduction

Magnetic mineral diagenesis involves the postdepositional modification of magnetic particles either by alteration of detrital sedimentary minerals or by authigenic growth of secondary magnetic minerals (Roberts, 2015). Diagenesis affects all sedimentary magnetic mineral assemblages, which makes it important to assess the extent of its effects. Diagenetic effects range from subtle (e.g., minor surficial oxidation of detrital/biogenic magnetic particles) to pervasive (e.g., complete dissolution of detrital/biogenic particles or growth of new authigenic phases that dominate the magnetic signal). Diagenetic magnetic mineral modification occurs over the full range of oxidizing to reducing conditions (Figure 1). Under oxic conditions, Fe^{2+} within magnetic minerals is oxidized progressively to Fe^{3+}. Under reducing conditions, Fe^{3+} within magnetic minerals is reduced to Fe^{2+}, which is achieved by corrosion of detrital/biogenic magnetic minerals, and incorporation of the liberated Fe^{2+} into authigenic pyrite or other paramagnetic phases. Reductive diagenesis is driven by microbial degradation of organic matter where different oxidants are used progressively with the following order of electron acceptor use: oxygen, nitrate, manganese oxides, iron (oxyhydr-)oxides, sulfate, and organic matter itself (Figure 1). When one oxidant is depleted, the next most efficient (i.e., most energy producing) oxidant is used, etc., until either all oxidants or all reactive organic matter are consumed (Froelich et al., 1979). In some settings, two respiration processes can occur simultaneously (e.g., Canfield & Thamdrup, 2009; Oremland & Taylor, 1978). The treatment provided here is based on the normal progression of environments expected during steady state diagenesis (Figure 1).

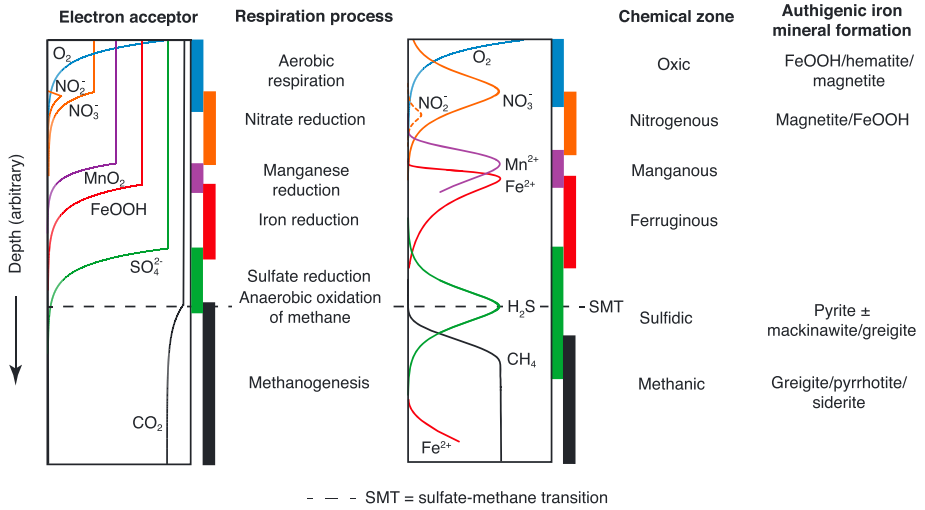

Figure 1. Cartoon representation of the depth distribution of sedimentary redox-driven diagenetic zones. Electron acceptors and respiration processes by which reactants are consumed are indicated on the left. Idealized pore water profiles of reactants (O_2, NO_2^-, and NO_3^-) and products (NO_3^-, Mn^{2+}, Fe^{2+}, H_2S, and CH_4) and associated chemical zones are shown on the right (modified from Jørgensen and Kasten (2006), Canfield and Thamdrup (2009), and Roberts (2015)). The names used for chemical zones are from Canfield and Thamdrup (2009). Authigenic iron minerals that can form in the respective chemical zones are listed in the far right-hand column (modified from Berner, 1981).

Magnetic minerals start to dissolve in ferruginous environments in association with iron reduction, and dissolution becomes pervasive in sulfidic environments where pore water sulfate is consumed entirely via microbial sulfate reduction or by anaerobic oxidation of methane (AOM) in underlying methanic environments, where the dominant process by which organic matter is degraded is via methanogenesis (Canfield & Thamdrup, 2009; Roberts, 2015). The ferruginous, sulfidic, and methanic diagenetic zones represent the more strongly reducing end of the spectrum in which the effects of diagenesis on magnetic mineral assemblages become pervasive. These environments are encountered frequently in paleomagnetic and environmental magnetic studies, which makes it important to have a thorough understanding of the types of magnetic mineral assemblages that occur in these settings and the diagenetic processes that modify or control them.

A key aim in rock magnetism over the last 20 years has been to develop techniques that enable identification of individual magnetic mineral components. This is important in most paleomagnetic and environmental magnetic applications where magnetic signals are carried by mixed magnetic mineral assemblages. For example, even in seemingly simple pelagic carbonate sediments, four or five distinct magnetic mineral components are identified commonly (Roberts et al., 2013). Each component can potentially carry valuable environmental information; being able to unmix rigorously the magnetic signals carried by such materials can unlock this environmental information. Magnetic unmixing is also valuable in paleomagnetic studies, where, for example, sedimentary relative paleointensity signals are recorded with different efficiency by cooccurring detrital and biogenic magnetite (Chen et al., 2017; Ouyang et al., 2014). Various unmixing methods have been developed, which generally involve fitting of functions to derivatives of isothermal remanent magnetization (IRM) acquisition or direct current demagnetization curves (e.g., Heslop & Dillon, 2007; Heslop et al., 2002; Kruiver et al., 2001; Robertson & France, 1994) or to alternating field demagnetization curves of an anhysteretic remanent magnetization or IRM (Egli, 2004a, 2004b, 2004c). A key issue with magnetic unmixing is that like any geophysical inversion method, potentially infinite combinations of components can be fitted to a given coercivity spectrum unless independent evidence is available concerning magnetic components (Heslop, 2015). So-called semisupervised or supervised unmixing is therefore needed to minimize ambiguities associated with spectral unmixing approaches (Heslop, 2015).

First-order reversal curve (FORC) diagrams (Pike et al., 1999; Roberts et al., 2000) are used widely in rock magnetism because of their diagnostic value in identifying magnetic domain states and magnetostatic interactions for magnetic mineral components (Roberts et al., 2014). FORC measurements provide information

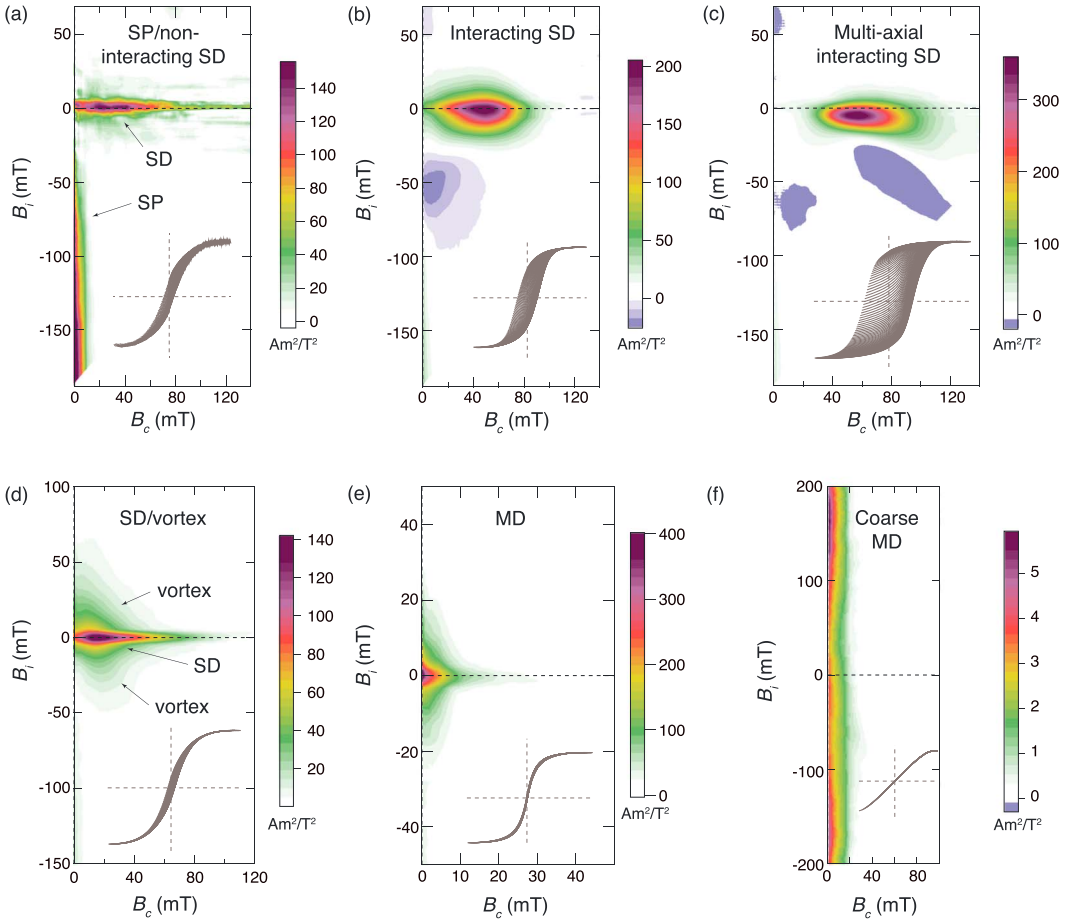

Figure 2. Representative FORC diagrams for fine magnetic particle systems with different dominant domain states. Examples are individual samples discussed later in this study, except (f). (a) Noninteracting SD particles with part of the particle assemblage near the SP/SD threshold size (see Pike, Roberts, and Verosub, 2001, for details). Sample MH30 from New Zealand, with the following VARIFORC smoothing parameters (Egli, 2013): $s_{c,0} = 8$, $s_{c,1} = 10$, $s_{b,0} = 7$, $s_{b,1} = 10$, and $\lambda_c = \lambda_b = 0.2$. Such diagenetically reduced samples are usually weakly magnetized and noisy. (b) Strongly interacting stable SD particles (see Pike et al. (1999) and Roberts et al. (2000, 2014) for details). Sample WB26 from New Zealand, with the following VARIFORC smoothing parameters (Egli, 2013): $s_{c,0} = 5$, $s_{c,1} = 7$, $s_{b,0} = 4$, $s_{b,1} = 7$, and $\lambda_c = \lambda_b = 0.1$. (c) Moderately magnetostatically interacting stable SD particles with multi-axial anisotropy (see Harrison and Lascu, 2014, for details). Sample SDC3950 from Italy, with the following VARIFORC smoothing parameters (Egli, 2013): $s_{c,0} = 5$, $s_{c,1} = 8$, $s_{b,0} = 5$, $s_{b,1} = 8$, and $\lambda_c = \lambda_b = 0.1$. (d) SD/vortex state particles (see Pike & Fernandez, 1999, and Roberts et al., 2017, for details). Sample CD1431056 from the Arabian Sea, with the following VARIFORC smoothing parameters (Egli, 2013): $s_{c,0} = 5$, $s_{c,1} = 8$, $s_{b,0} = 5$, $s_{b,1} = 8$, and $\lambda_c = \lambda_b = 0.1$. (e) MD particles typically seen in natural samples (Roberts et al., 2000; Pike, Roberts, Dekkers, et al., 2001). Sample NR27 from New Zealand, with the following VARIFORC smoothing parameters (Egli, 2013): $s_{c,0} = 5$, $s_{c,1} = 7$, $s_{b,0} = 4$, $s_{b,1} = 7$, and $\lambda_c = \lambda_b = 0.1$. (f) MD particles seen in coarser systems dominated by domain wall pinning (see Pike, Roberts, Dekkers, et al., 2001, and Roberts et al., 2014, for details). Geological samples rarely have such behavior; the example is a silicon steel sample with conventional FORC smoothing with smoothing factor = 4. The respective sets of measured FORCs are shown as gray insets in the lower part of each panel.

about the magnetic response of all particles in a sample in terms of magnetization (represented by the magnitude of the FORC distribution), and the coercivity and magnetic interaction field distributions (B_c and B_i axes of the FORC diagram, respectively), where contrasting features can be used to diagnose the full range of magnetic domain states in fine magnetic particle systems. FORC distributions are therefore powerful for exploring subtle magnetization processes that are unrecognizable in standard hysteresis measurements. For readers who are less familiar with FORC diagrams, we show typical FORC diagrams in Figure 2 and refer here to papers that describe the key features for the following types of particle systems: superparamagnetic (SP; Pike, Roberts, & Verosub, 2001), stable single domain (SD) with and without

interactions (Pike et al., 1999; Roberts et al., 2000, 2014), vortex (Pike & Fernandez, 1999; Roberts et al., 2000, 2017; Muxworthy & Dunlop, 2002), and multidomain (MD; Pike, Roberts, Dekkers, et al., 2001). Despite their widespread use, most applications of FORC diagrams have only involved qualitative domain state identification or quantitative assessment of interactions (e.g., Carvallo et al., 2006; Muxworthy & Dunlop, 2002) without quantifying the contributions from each magnetic mineral component present in a sample, although some more quantitative attempts have had limited success (Muxworthy et al., 2005). This situation has changed with development of tools that enable quantitative simulation of FORC distributions (Harrison & Lascu, 2014) and with introduction of principal component analysis (PCA) to unmix FORC distributions (Heslop et al., 2014) into end-member (EM) components (Lascu et al., 2015). An important aspect of unmixing is to solve the linear mixing equation (Heslop, 2015), which was not achieved in the FORC-PCA approach of Lascu et al. (2015). Harrison et al. (2018) therefore further developed FORC unmixing to solve this equation.

In this paper, we use the new FORC unmixing algorithm of Harrison et al. (2018), which is built into the FORCinel software package (Harrison & Feinberg, 2008), to illustrate its power for understanding magnetic particle assemblages in sedimentary sequences that have undergone reductive diagenesis. Our aim is to reveal diagenetic processes through identification of the magnetic minerals present in these diagenetic systems. The identified magnetic components should be useful for future studies of similar diagenetic environments in which these components are expected to be encountered, where FORC unmixing can enable quantitative assessment of their respective contributions. Typical FORC diagrams for each domain state shown in Figure 2 can be used as a guide to EM interpretation in the discussion below.

2. Methods

The FORC measurements used in this study were all made with Princeton Measurements Corporation vibrating sample magnetometers in various laboratories around the world, with averaging times of 250 ms. The sample collections subjected here to FORC unmixing were treated with VARIFORC processing (Egli, 2013), where the parameters used are indicated in the respective figure captions for each data set presented.

While progressive reductive diagenesis might be expected to transform an initially more complex detrital/biogenic magnetic particle assemblage into one with simpler and less variable magnetic properties with either weak relict or authigenically enhanced magnetizations, we treat most sample sets independently. This approach maintains the integrity of the respective sample sets, and it recognizes an important limitation associated with visualization of unmixing results. Multiple-component systems are readily represented in binary mixing lines, ternary diagrams, or in tetrahedra for quaternary mixtures, but higher-order mixing becomes more difficult to represent. This is not because of the mathematics, which can cope with many components, but because of the difficulty in visualizing results for so many components. Treating each sample set independently reduces the number of components identified, which helps to simplify data visualization.

2.1. The New FORC Unmixing Algorithm

PCA is used routinely in many disciplines to estimate unknown EMs by providing a low-rank approximation to data that facilitates definition of an empirical mixing space (Heslop, 2015). Details of FORC unmixing are described by Harrison et al. (2018); a brief outline is provided here to help readers to understand essential aspects of the approach. The principal advance in the FORC unmixing algorithm of Harrison et al. (2018) compared to that of Lascu et al. (2015) is that PCA is now performed on a representation of the magnetization curves rather than on processed FORC diagrams: this enables identification of both irreversible (i.e., remanence-bearing) and reversible magnetization components so that the total magnetization is the sum of linearly additive components that satisfy the linear mixing equation. With this approach, contributions due to SP and MD components, which either have no or little irreversible magnetization, are recognized and quantified. With the graphical user interface available in FORCinel (Harrison & Feinberg, 2008), EMs can be visualized and selected interactively using the FORC-PCA algorithm. EM selection is not physically constrained and is based on user selection; best solutions are obtained when users have other constraints with which to "supervise" EM selection. To facilitate EM selection, newly devised feasibility metrics are included to define an unmixing space within which EMs are physically realistic (Harrison et al., 2018). The feasibility metrics are contoured to help users to select EMs that satisfy reasonable criteria such as requiring FORCs to change monotonically and to not cross each other. Demarcation of this

physically realistic space helps users to avoid manual selection of unrealistic EMs. Even with these feasibility constraints, EM selection within the "allowable space" depends on the user. It is generally desirable to select EMs that lie close to measured data points, but an EM can also represent a mixture (e.g., Heslop, 2015), so it can be desirable to select an EM that lies further from measured data points to obtain a less mixed EM. These aspects of EM selection are subjective, which emphasizes the need for independent information about samples and the value of user expertise.

Smoothing of measurement noise is a key challenge for FORC processing (Egli, 2013; Harrison & Feinberg, 2008; Roberts et al., 2000, 2014). To ensure that results for EMs and individual samples are comparable, all samples within a given data set are treated in the FORC-PCA approach with the same VARIFORC parameters. This poses particular challenges when studying diagenesis because signal/noise ratios will contrast strongly because sample sets tend to contain either typical detrital or diagenetically enhanced magnetic mineral assemblages along with diagenetically depleted assemblages. This issue is discussed below where relevant. Following Egli (2013), areas where the FORC distribution equals zero are white. The positive FORC signal is then scaled from zero to the maximum value, and the negative region is scaled to its highest negative value. As discussed below, negative regions are important; more blue shades are evident when a negative region is deeper than for shallow negative regions.

While FORC unmixing has significant strengths, it also has limitations. The unmixing approach is as good as the data fed into it. For example, in the present study, FORC measurements focus on the $<$120 mT coercivity range. This biases explicitly against visualization of high coercivity minerals such as hematite and goethite. The weak spontaneous magnetizations of these minerals can also be swamped by more strongly magnetic coexisting minerals such as magnetite in FORC diagrams (e.g., Muxworthy et al., 2005; Roberts et al., 2014). Hematite tends to have broad coercivity spectra that extend from low to high values, so hematite will usually be partially evident in FORC diagrams with the field ranges used in this study (Roberts et al., 2006). As shown by Zhao et al. (2017), its detection can still be difficult when magnetite is present, and visualization of a hematite component is facilitated by use of adjustable nonlinear color maps for FORC diagrams. Goethite has exceptionally high coercivity (Rochette et al., 2005), which makes it generally invisible in FORC diagrams in the adopted $<$120 mT coercivity range (cf. Roberts et al., 2006). Semiquantitative determination of hematite and goethite concentrations is better achieved with low-temperature magnetic measurements (e.g., Lagroix & Guyodo, 2017). Our aim here is to understand diagenetic effects on typical detrital magnetic mineral assemblages and authigenic magnetic minerals that form during reductive diagenesis. Limitations associated with recognizing hematite and goethite are acknowledged, and readers with interests in understanding the diagenetic fate of these minerals should bear in mind that they will be largely invisible in the data representations in this paper. Overall, quantitative FORC analysis enabled by FORC unmixing has considerable potential because the domain state and interaction field distribution can be identified for each constituent magnetic component, which provides unprecedented levels of valuable information even for samples that comprise complex magnetic mixtures.

3. Samples and Setting

We present here reanalyzed FORC data from several of our own published studies of reductive magnetic mineral diagenesis. We use well-studied sample sets so that the identified components are known and can be used as references for such diagenetic systems in future studies. The studied samples include modern depositional systems in which detrital/biogenic magnetic mineral assemblages at the seafloor undergo progressive magnetic property changes associated with down-core reductive dissolution. This type of environment is represented by hemipelagic sediments recovered in sediment cores CD143-55705 from the Oman margin, Arabian Sea (Chang, Heslop, et al., 2016; Rowan et al., 2009), and LC13-81-G138 from the Northern California margin, Pacific Ocean (Rowan et al., 2009). These cores progress from the oxic to methanic diagenetic zones and are dominated by sulfidic diagenesis (see Figure 1 and Roberts (2015) for nomenclature). Sulfidic to methanic diagenetic systems with more complete diagenetic reduction are represented by tectonically uplifted marine sediments from Neogene sequences that crop out throughout eastern North Island, New Zealand (Rowan & Roberts, 2006); Pleistocene marine sediments from Crostolo River, Italy (Roberts et al., 2005); and middle Pleistocene alluvial sediments from a drill core on the Tiber River coastal plain near Rome, Italy (Florindo et al., 2007). Methanic environments are represented by sediment cores from Hydrate

Ridge, Cascadia margin, offshore of Oregon, USA, which were recovered during Ocean Drilling Program (ODP) Leg 204 (Larrasoaña et al., 2007).

4. Results

4.1. Progressive Down-Core Dissolution: Ferruginous to Sulfidic Diagenesis

Many studies of coastal, hemipelagic, and pelagic sediments document progressive down-core diagenetic dissolution of detrital iron oxides in reducing environments (Bouilloux et al., 2013; Chang, Bolton, et al., 2016; Channell & Hawthorne, 1990; Dillon & Bleil, 2006; Emiroglu et al., 2004; Garming et al., 2005; Karlin, 1990a, 1990b; Karlin & Levi, 1983, 1985; Kawamura et al., 2007; Leslie, Hammond, et al., 1990; Leslie, Lund, et al., 1990; Liu et al., 2004; Mohamed et al., 2011; Rey et al., 2005; Richter et al., 1999; Riedinger et al., 2005; Roberts, 2015; Roberts & Turner, 1993; Robinson et al., 2000; Rowan et al., 2009; Yamazaki et al., 2003). These studies provide a common picture of surface sediments, generally with all stages of organic matter diagenesis recognized in pore water profiles (Figure 1; Roberts, 2015). Surface sediments generally contain trace abundances of detrital iron oxide minerals, including ferric oxyhydroxides and biogenic magnetite. With ongoing burial, reactive magnetic minerals start to undergo dissolution in ferruginous diagenetic environments and more pervasive dissolution occurs once sulfide is produced in pore waters, with the finest particles dissolving first, and pyrite becoming increasingly abundant in sulfidic environments. The depth at which the magnetic mineral content declines precipitously depends on the organic carbon content and sedimentation rate and can vary significantly (e.g., Karlin & Levi, 1983; Kawamura et al., 2007; Roberts, 2015). We provide below two examples of FORC unmixing in environments that progress through the ferruginous and sulfidic diagenetic stages (Figure 1).

4.1.1. Core CD143-55705, Oman Margin

FORC unmixing results are shown in Figure 3 for 50 samples from core CD143-55705. This core has been studied extensively in relation to magnetic mineral diagenesis (Chang, Heslop, et al., 2016; Rowan et al., 2009) and is used here to illustrate diagenetic alteration of surface magnetic mineral assemblages. High initial IRM values (Figure 3j, gray curve) associated with a surface detrital/biogenic magnetic mineral assemblage decrease in two sharp steps at depths of ~2 and ~4.2 m to low values below ~5 m. The large IRM contrast between the upper and lower parts of the core presents a challenge for calculating FORC distributions because of the variable signal/noise ratio and the need to smooth FORCs more for weakly magnetized samples. This challenge is illustrated in Figures 3a and 3b, where data are presented with respect to three principal components (PCs). In Figure 3a, data are plotted in the PC1-PC2 plane where it is clear that data from the upper part of the core (above ~4.2 m) fall on a single trend and data from the lower part of the core are scattered. Data that fall on a linear trend with positive PC1 values and near-zero PC2 values in Figure 3a for the upper part of the core define a triangular region in the PC1-PC3 plane in Figure 3b, where data from the lower part of the core (below ~4.2 m) are also scattered. Therefore, we treat separately data from the upper and lower parts of the core. The triangular region identified in the PC1-PC3 plane in Figure 3b is used to define a three-EM system for the upper part of the core, where FORC diagrams for the three EMs are shown in Figures 3d–3f and the vertices of the triangle that represent each EM are shown with respect to the data in Figure 3g. As should be the case for a physically meaningful solution, the triangle for the three-EM mixing system falls within a broader zone enclosed by shaded contours (Figure 3g) in which FORCs increase monotonically without crossing each other (Harrison et al., 2018). Noisier data from the lower part of the core are treated separately and are represented in the PC1-PC2 plane in Figure 3h. The conventional unmixing procedure is to define a mixing region in PC space from which EMs are identified. Due to the noisy nature of the data, we chose a single component that represents the entire magnetic mineral assemblage for the lower part of the core. With this approach, the scatter in the PC1-PC2 plane is considered to be due to the noisy data for weakly magnetized samples rather than due to a mixed magnetic mineral assemblage. A FORC diagram for this component is shown in Figure 3i, which is represented by the point where PC1 and PC2 equal zero (Figure 3h). An equivalent approach would be to average all FORC measurements from this interval to improve the signal/noise ratio.

The three components identified in the upper part of core CD143-55705 (Figures 3d–3f) are represented by a stable SD/fine vortex state component (EM1), a coarse vortex state/MD component (EM2), where vortex states are identified following the arguments of Roberts et al. (2017), and a noisier SP to SD component (EM3). Down-core variations for the three components identified for the upper part of the core are shown in Figure 3j. EM1 is dominant in the uppermost part of the core, where the sharp noninteracting central ridge

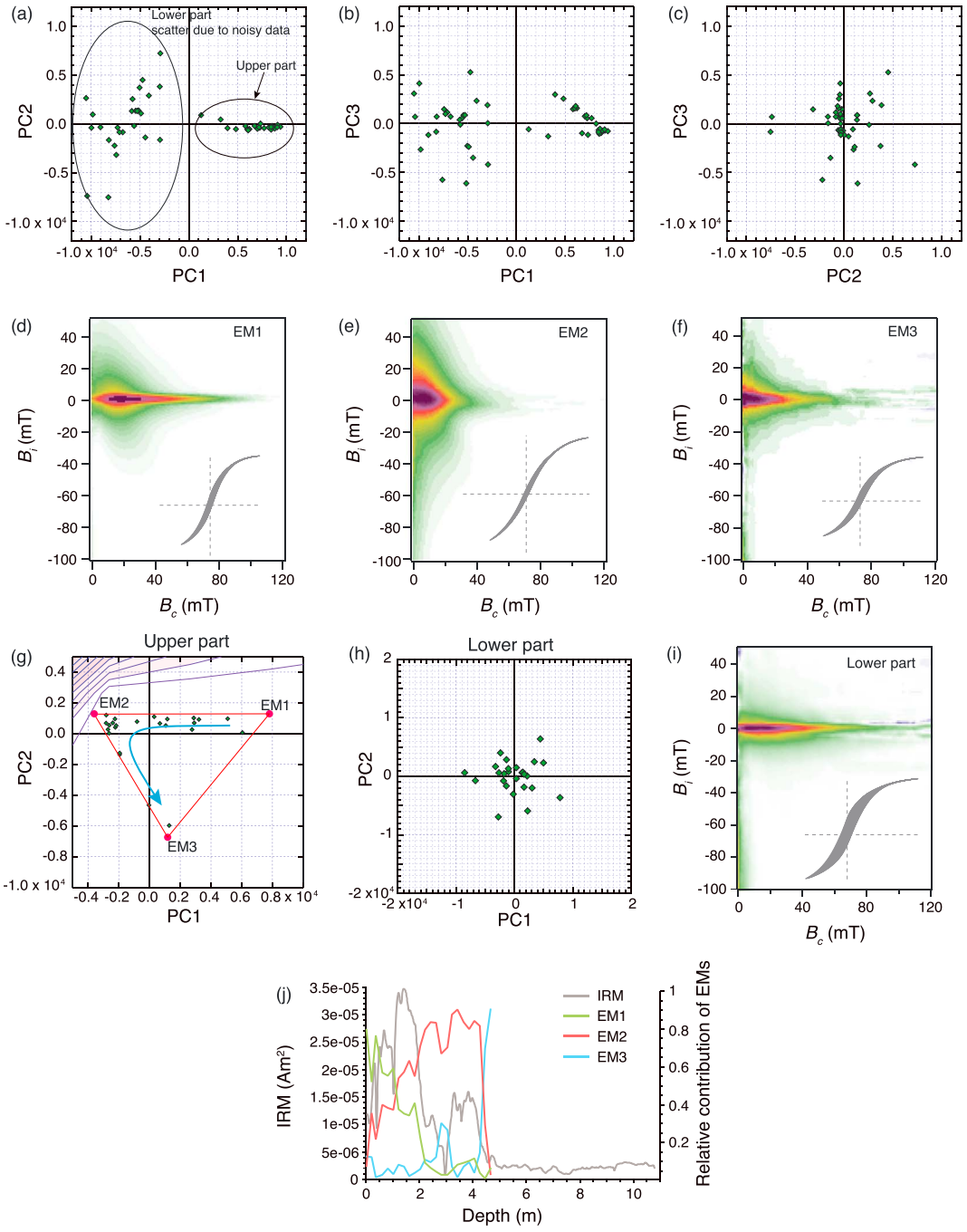

Figure 3. FORC unmixing results for ferruginous to sulfidic diagenetic environments in core CD143-55705. Distribution of PCs for 50 measured FORC diagrams in (a) PC1-PC2 space, (b) PC1-PC3 space, and (c) PC2-PC3 space. Data for the lower part of the core (enclosed by an ellipse in (a)) are noisy and are treated separately (26 samples). Data for the upper part of the core (enclosed by an ellipse in (a); 24 samples) define a triangular region in (b) from which three EMs are defined where (d) is a noninteracting stable SD/vortex state component (EM1) due to biogenic and detrital magnetite, (e) is a coarser vortex state to MD component (EM2) due to detrital magnetic minerals, and (f) is an authigenic SP-SD component (EM3) that formed during early diagenesis. Sets of FORCs shown for EMs in this and other figures are usually incomplete representations. For experimental measurements, a set of FORCs provides an outline of the major hysteresis loop and is approximately symmetrical, whereas the lower part of the set of FORCs for EMs is usually not shown because the lowermost FORCs represent areas that lie outside the limits defined for the EM FORC diagrams. In such a representation, EM FORCs will, thus, usually appear truncated and asymmetrical and can possibly appear distorted. The triangular mixing space with positions of the three EMs is shown in (g), where contours indicate the space where FORC distributions start to become physically unrealistic (see Harrison et al., 2018). The arrow indicates the general down-core trend from EM1 to EM2 to EM3. (h) Representation of the noisy data from the lower part of the core (ellipse in (a)) that were averaged to obtain (i) a FORC diagram defined where PC1 and PC2 equal zero in (h). (j) Down-core IRM profile (gray) with relative contributions of EM1, EM2, and EM3. VARIFORC parameters (see Egli, 2013) for smoothing of the PCA solution are: $s_{c,0} = 5$, $s_{c,1} = 8$, $s_{b,0} = 5$, $s_{b,1} = 8$, and $\lambda_c = \lambda_b = 0.1$. The maximum applied field for FORC measurements was 500 mT, which is sufficient to saturate magnetically the low-coercivity minerals in the studied samples.

signal is interpreted to be due to biogenic magnetite (cf. Egli et al., 2010; Roberts et al., 2012). EM1 also has a fine vortex state detrital contribution. Chang, Heslop, et al. (2016) demonstrated that biogenic and detrital magnetite record the low-temperature Verwey transition at different temperatures and that biogenic magnetite is present in this core to depths of 4.60 m. This interpretation is consistent with the down-core profile for EM1 in Figure 3j. EM2 represents a coarser detrital magnetic mineral fraction whose relative importance increases to depths of ~4.6 m at which point it drops sharply. EM3 is interpreted to represent an authigenic SP/SD component that has trivial relative concentrations in the upper part of the core except for within the minimum between two IRM peaks (Figure 3j). Its relative importance also increases sharply at ~4.6 m. The contribution from EM1 drops at the base of the upper IRM peak, and EM2 is responsible for all of the lower IRM peak, and EM3 is always weak. The FORC diagram for EM3 (Figure 3f) is indicative of an SP/SD greigite assemblage and is similar to the average FORC result for the lower part of the core (Figure 3i), except that the latter has a greater stable SD contribution and a lesser SP contribution. Interpretation of these trends in terms of diagenesis is discussed further below.

4.1.2. Core LC13-81-G138, Northern California Margin

FORC unmixing results are shown in Figure 4 for core LC13-81-G138 (15 samples). This core has also been studied previously in relation to magnetic mineral diagenesis (Rowan et al., 2009). Contrasting magnetizations in the upper and lower, diagenetically depleted, parts of the core mean that these two intervals are treated separately, as we did for core CD143-55705. Two data clusters occur in the PC1-PC2 plane (Figure 4a): a tight cluster at PC1 $\approx 1 \times 10^{-4}$ and a noisy one at PC1 < 0. In the PC1-PC3 plane (Figure 4b), the cluster at PC1 $\approx 1 \times 10^{-4}$ has a wider distribution along a line at constant PC1 values. This trend defines a binary mixing line (Figure 4g) where EM1 is represented by a noninteracting stable SD component with a strong central ridge (Figure 4d) that is typical of biogenic magnetite (e.g., Egli et al., 2010; Roberts et al., 2012), and EM2 is a coarse detrital component dominated by the vortex state (Figure 4e). The measured data lie closer to EM2, and selection of EM1 in a position some distance away from the measured data (Figure 4g) is done to isolate an EM with a pure central ridge signature (Figure 4d) without admixture of EM2 (Figure 4e). Identical EM1 and EM2 components were identified by Channell et al. (2016), which they also identified as due to biogenic and detrital magnetite, respectively. Again, instead of fitting multiple components to the noisy FORC distributions from the lower part of the core, a single FORC distribution is selected to represent this interval (Figure 4f) where PC2 and PC3 equal zero (Figure 4c).

As is the case for core CD143-55705, the upper part of core LC13-81-G138 is dominated by SD biogenic and coarser detrital magnetite components. This biogenic component declines throughout the upper part of the record at the expense of the coarser detrital component in both cores LC13-81-G138 (Figure 4i) and CD143-55705 (Figure 3j). The diagenetically depleted lower part of core LC13-81-G138 (Figure 4f) has a similar average SP/SD FORC signature as the same zone in core CD143-55705 (Figure 3i). Interpretation of the LC13-81-G138 record in terms of diagenesis is discussed further in section 5.

4.2. Magnetic Enhancement Via Greigite Authigenesis: Sulfidic Diagenesis

In the examples discussed above, reductive diagenesis has depleted initial surficial detrital/biogenic magnetic mineral assemblages via dissolution, followed by weak magnetic enhancement via authigenic growth of SP/SD greigite. During early diagenesis, dissolved Fe^{2+} and H_2S react to form authigenic greigite, which can grow from initially fine SP/SD assemblages to stable SD particle assemblages with strong magnetostatic interactions that dominate magnetic mineral assemblages. Greigite can also grow in methanic environments in association with AOM. We now consider greigite-forming environments with two sets of examples.

4.2.1. Greigite Formation in Pleistocene Sediments From Italy

4.2.1.1. Middle Pleistocene Alluvial Sediments, Tiber River Plain

We present results here for middle Pleistocene alluvial sediments from a drill core on the Tiber River plain near Rome, Italy (Florindo et al., 2007). Harrison et al. (2018) used FORC results from this group of 16 samples to illustrate FORC unmixing, which we show in Figure 5. Three EMs are identified, all of which are due to greigite. EM1 (Figure 5a) has less vertical spread than EM2 (Figure 5b), and a negative peak that starts from below the main positive peak of the FORC distribution with a trend at $-45°$ from the positive peak (Figure 5a). EM2 has a strong positive contribution with a broad, concentric distribution, and a deeper negative contribution along the negative B_i axis (Figure 5b) that is typical of interacting SD greigite (Roberts et al., 2006, 2011). EM3 comprises a SP/SD component (Figure 5c) that is present in all sample sets analyzed here. FORC measurements

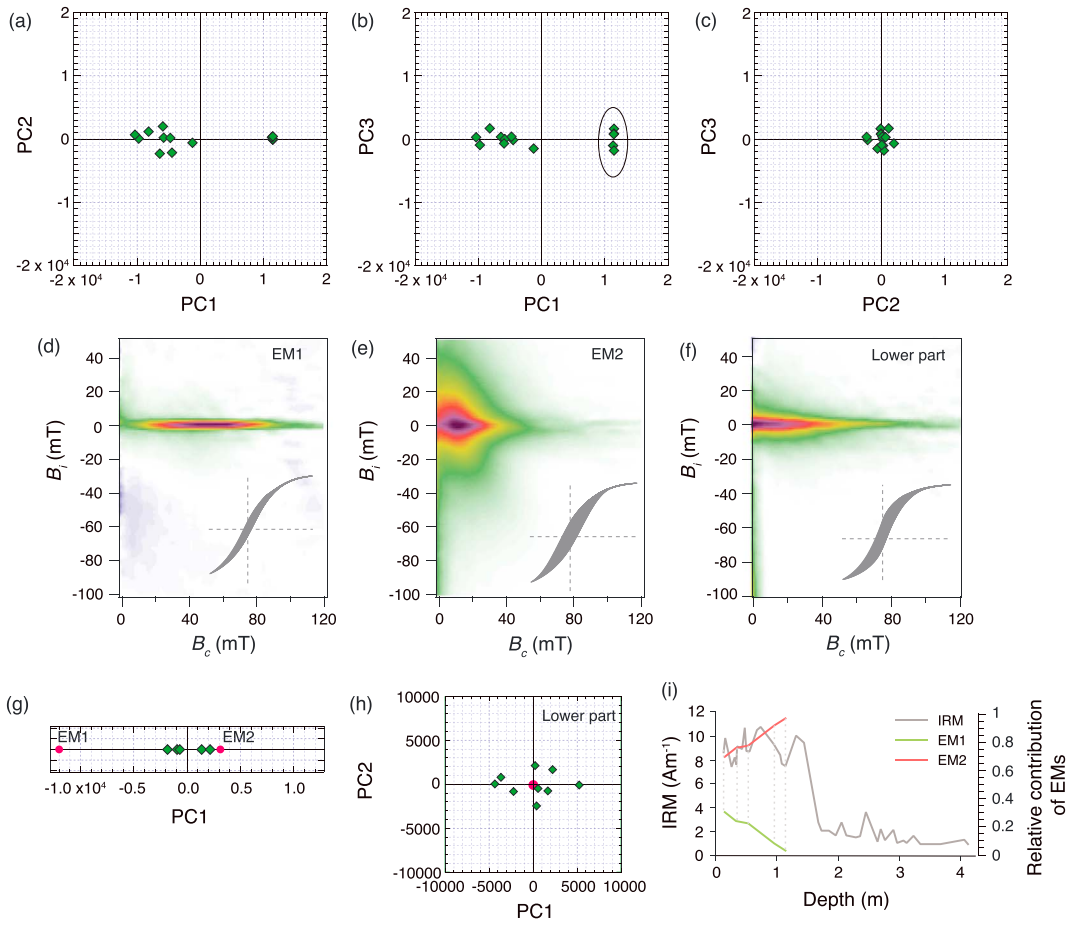

Figure 4. FORC unmixing results for ferruginous to sulfidic diagenetic environments in marine sediment core LC13-81-G138. Distribution of PCs for 15 measured FORC diagrams in (a) PC1-PC2 space, (b) PC1-PC3 space, and (c) PC2-PC3 space for core LC13-81-G138. Data for the lower part of the core (scattered data to the left in (a) and (b)) are noisy and are treated separately (10 samples). Data for the upper part of the core (enclosed by an ellipse in (b); five samples) define a binary mixing line from which two EMs are defined where (d) is a noninteracting stable SD component (EM1) due to biogenic magnetite and (e) is a coarser vortex state component (EM2) due to detrital magnetic minerals. (f) An authigenic SP-SD component (EM3) that formed during early diagenesis is obtained by averaging the noisy FORC data indicated in (h) where PC1 and PC2 equal zero. (g) Binary mixing space with positions of two EMs for the upper part of the core. (i) Down-core IRM profile (gray) with relative contributions of EM1 and EM2 for the upper part of the core. VARIFORC parameters (see Egli, 2013) for smoothing of the PCA solution are $s_{c,0} = 5$, $s_{c,1} = 8$, $s_{b,0} = 5$, $s_{b,1} = 8$, and $\lambda_c = \lambda_b = 0.1$. The maximum applied field for FORC measurements was 500 mT, which is sufficient to saturate magnetically the low-coercivity minerals in the studied samples.

for four weakly magnetized samples were averaged to increase the signal/noise ratio to obtain an average result that was included in the PCA to identify EM3. The identified three-EM system is defined within the contoured region for physically realistic solutions in the PC1-PC2 plane (Figure 5d). Typical FORC diagrams for real samples are shown for comparison with the calculated EMs in Figures 5e–5h. These samples are dominated by EM2 (Figures 5g and 5h) but also clearly represent mixtures with the other EMs (Figures 5e and 5f). Details of the EMs and the processes that they represent are discussed further below.

This example also illustrates challenges associated with FORC unmixing. The horizontal stripes in FORC diagrams for EM2 and EM3 are due to VARIFORC smoothing (Egli, 2013), where the unmixing space is defined using noisy experimental data and the same VARIFORC parameters are used to unmix the entire sample set (Harrison et al., 2018). These "stripes" are mostly present in weak samples or EMs. The weak EM3 is dominated by a horizontal ridge; measurement noise coupled with the chosen VARIFORC parameters produces the artifact stripes. Despite the visually and technically unappealing artifact stripes associated with FORC smoothing for weakly magnetized samples and calculated EMs, the overall FORC pattern is clear.

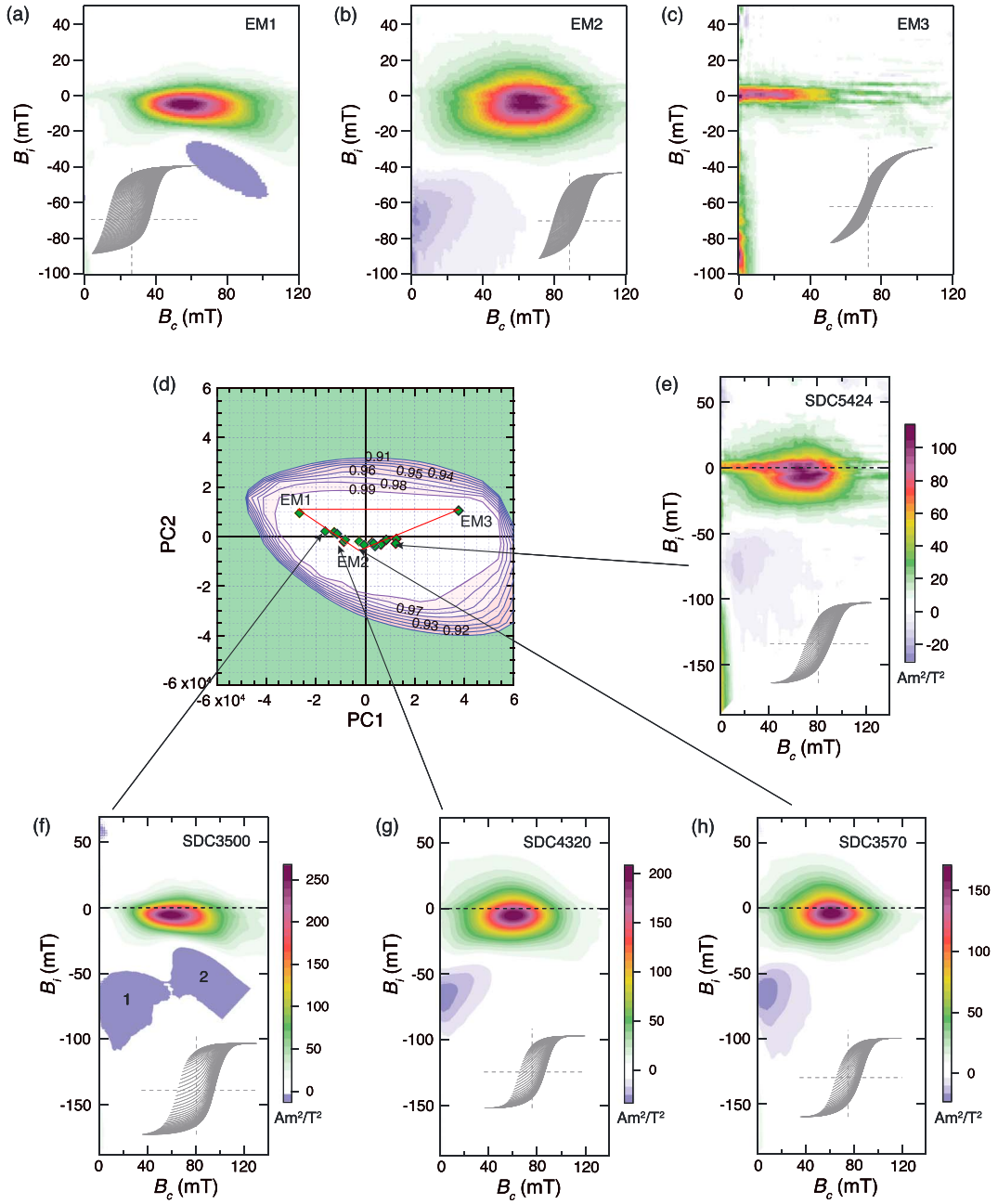

Figure 5. FORC unmixing results for sulfidic diagenetic environments in middle Pleistocene Italian fluvial clays (Florindo et al., 2007). (a) EM1 is magnetostatically interacting stable SD greigite, where the negative region at −45° is indicative of multiaxial anisotropy (see Harrison and Lascu (2014)). (b) EM2 is a magnetostatically interacting stable SD greigite component with higher coercivity than EM1. (c) EM3 is an authigenic SP-SD component that is observed in all environments analyzed here (defined by the average for four weakly magnetized samples). (d) The triangular mixing space with positions of the three EMs for 16 samples, where the contours indicate the space where FORC distributions start to become physically unrealistic. (e–h) FORC diagrams for measured samples, which fall dominantly near (g and h) EM2, with mixtures with (e) EM3 and (f) EM1. VARIFORC parameters (see Egli, 2013) for smoothing of the PCA solution are $s_{c,0} = 8$, $s_{c,1} = 10$, $s_{b,0} = 7$, $s_{b,1} = 10$, and $\lambda_c = \lambda_b = 0.1$. The maximum applied field for FORC measurements was 500 mT, which is sufficient to saturate magnetically the low-coercivity minerals in the studied samples.

Smoothing of noisy measurement data is a key challenge in FORC data processing (e.g., Egli, 2013; Harrison & Feinberg, 2008; Roberts et al., 2000, 2014); this example illustrates some of the compromises associated with the second derivative calculation used to obtain FORC distributions.

4.2.1.2. Lower Pleistocene Marine Sediments, Crostolo River

We present results here for tectonically uplifted lower Pleistocene greigite-bearing marine sediments from Crostolo River, Italy (Roberts et al., 2005; Tric et al., 1991). Three EMs are identified from 12 analyzed samples (Figures 6a–6c), which are similar to those from the Tiber River plain, with two distinct interacting SD components (EM1 and EM2; Figures 6a and 6b) and one SP/SD component (EM3; Figure 6c). In PC1-PC2 space, most data points cluster around EM2 (Figure 6e), so that measured FORC diagrams are mainly like those of EM2 (Figure 6f). Only four data points reveal more scatter (Figures 6d and 6e); these samples represent mixtures of the three identified EMs, where sample CR01B (Figure 6i) is a mixture of EM2 and EM3, sample CR03B is closer to EM1 (Figure 6g), and sample CR02D lies closest to EM3 but has contributions from both EM1 and EM2 (Figure 6h). Like the Tiber River plain example, the three EMs are all authigenic components that grew during diagenesis, as discussed further below.

4.2.2. Greigite Formation in Neogene Marine Sediments, New Zealand

We present results here for tectonically uplifted Neogene marine sediments that crop out throughout eastern New Zealand (Rowan & Roberts, 2006). We group FORC results for 129 samples from wide-ranging mudstone outcrops of varying age because they appear to have undergone diagenesis in similar environments. Four EMs are identified from FORC unmixing (Figure 7). These sediments have been altered strongly by reductive diagenesis, but a detrital magnetic component persists in some tuffaceous samples, and iron-titanium oxides are also likely to occur as inclusions within detrital silicate particles (Chang, Roberts, et al., 2016). EM1 is identified as a coarse detrital iron oxide MD component carried by four tuffaceous samples from the NR locality of Rowan and Roberts (2006) (Figure 7a). By contrast, EM2 is represented by pure SD greigite with strong magnetostatic interactions (Figure 7b), that is a typical signature of authigenic greigite (e.g., Chang et al., 2014; Florindo et al., 2007; Liu et al., 2016; Roberts et al., 2006, 2011; Rowan & Roberts, 2006; Vasiliev et al., 2007). EM3 and EM4 link the other two components (Figures 7e and 7f), where both have a strong SP signal but EM3 contains a SD/vortex state detrital fraction (Figure 7c), while EM4 comprises a less strongly interacting SP/SD greigite component (Figure 7d). These four components are typical of the New Zealand sediments studied by Rowan and Roberts (2006). Mixing among the four EMs is illustrated in Figures 7e and 7f, and FORC diagrams for typical samples with intermediate properties are shown in Figures 7g–7j. Details of the EMs and the processes that they represent are discussed further below.

4.3. Magnetic Mineral Diagenesis in Methanic Environments

Methanic environments are represented by sediment cores from Hydrate Ridge, Cascadia margin, offshore of Oregon, USA, which were recovered during ODP Leg 204 (Larrasoaña et al., 2007). FORC diagrams for 20 samples can be represented by four components (Figure 8), the first three of which are common to sulfidic environments (Figures 5 and 6). EM1 is a coarse vortex state component due to detrital magnetic minerals (Figure 8a), which is associated with terrigenous inputs via turbidites (Larrasoaña et al., 2007). EM2 is a strongly magnetostatically interacting SD greigite component (Figure 8b), while EM3 corresponds to the authigenic SP/SD component that is seen in all examples above (Figure 8c). EM4 (Figure 8d) is typical of methanic environments and is due to authigenic pyrrhotite (e.g., Horng, 2018; Kars & Kodama, 2015a, 2015b; Larrasoaña et al., 2007; Roberts et al., 2010; Weaver et al., 2002). Relationships among the EMs for this data set are shown in Figures 8e and 8f. Typical FORC diagrams for intermediate samples that fall between EMs are shown in Figures 8g and 8h. The EM2-EM3 trend represents the dominant variation between fine SP/SD greigite and stable SD greigite assemblages. EM1 represents an isolated component where coarse detrital particles have been admixed via exogenous turbidite inputs, while EM4 represents an additional authigenic pyrrhotite component that has formed during methanic diagenesis. Details of the EMs and the processes that they represent are discussed further below.

5. Discussion

5.1. Domain States and Magnetocrystalline Anisotropy Types in EMs

Expected FORC signatures for all domain states (Figure 2) can be compared with those identified for each EM in Figures 3–8. When using PCA, any EM can represent a mixture of magnetic components (Heslop, 2015),

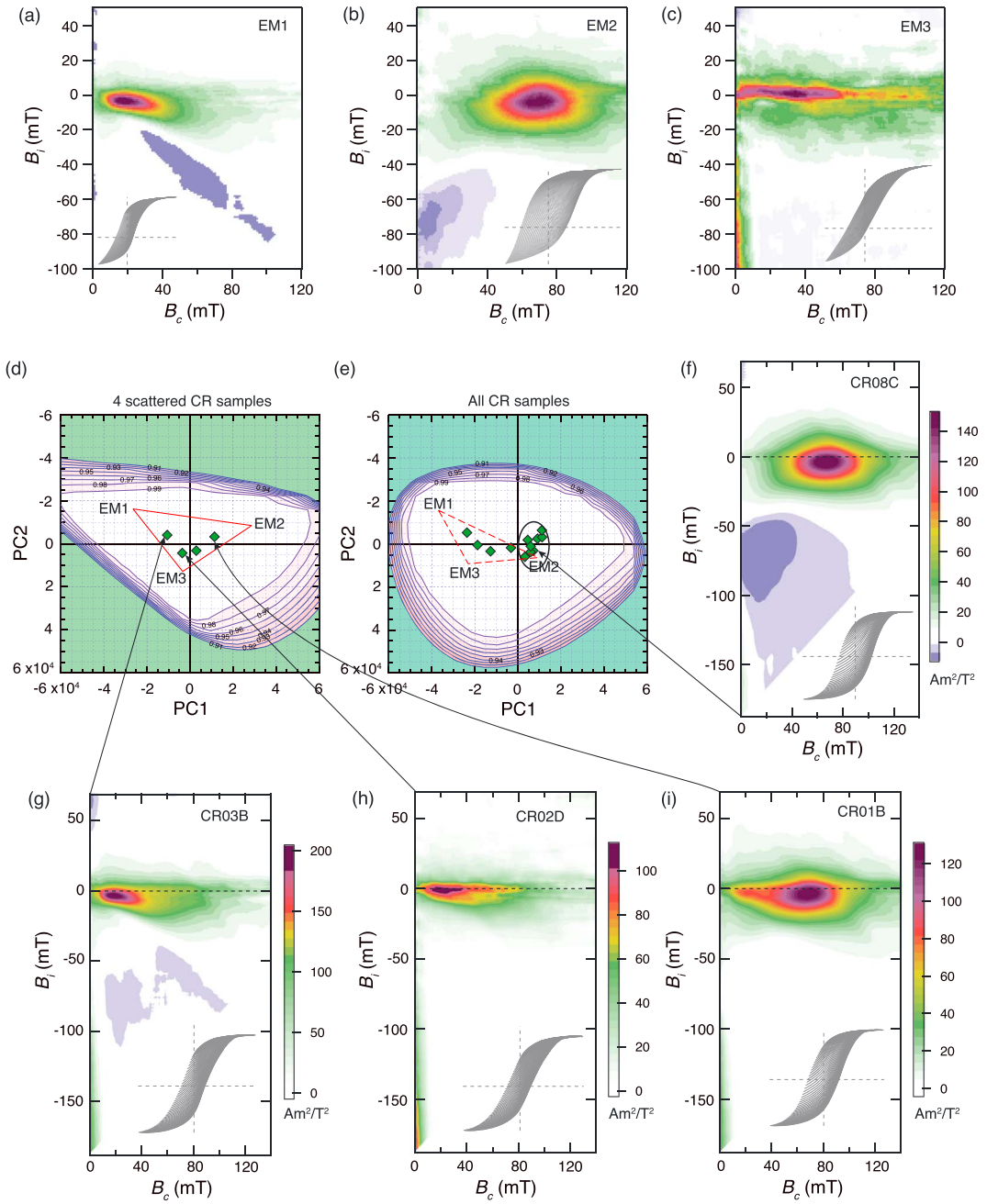

Figure 6. FORC unmixing results for sulfidic (and methanic) diagenetic environments in tectonically uplifted lower Pleistocene marine mudstones from Crostolo River, Italy (Roberts et al., 2005). (a) EM1 represents magnetostatically interacting pyrrhotite, where the negative region at −45° is indicative of multiaxial anisotropy (see Harrison & Lascu, 2014). (b) EM2 is a magnetostatically interacting stable SD greigite component. (c) EM3 is an authigenic SP-SD component that is observed in all environments analyzed here. (d and e) Triangular PC1-PC2 mixing space (12 samples) with (d) four scattered weakly magnetized samples from which three EMs are defined and (e) all samples, where the dominant behavior is scattered around EM2. Contours in (d and e) indicate the space where FORC distributions start to become physically unrealistic. (f–i) FORC diagrams for measured samples, which range from (f) being dominated by EM2, (g) near EM1, (h) a mixture of EM1 and EM3, and (i) a mixture of EM2 and EM3. VARIFORC parameters (see Egli, 2013) for smoothing of the PCA solution are $s_{c,0} = 8$, $s_{c,1} = 10$, $s_{b,0} = 7$, $s_{b,1} = 10$, and $\lambda_c = \lambda_b = 0.1$. The maximum applied field for FORC measurements was 500 mT, which is sufficient to saturate magnetically the low-coercivity minerals in the studied samples.

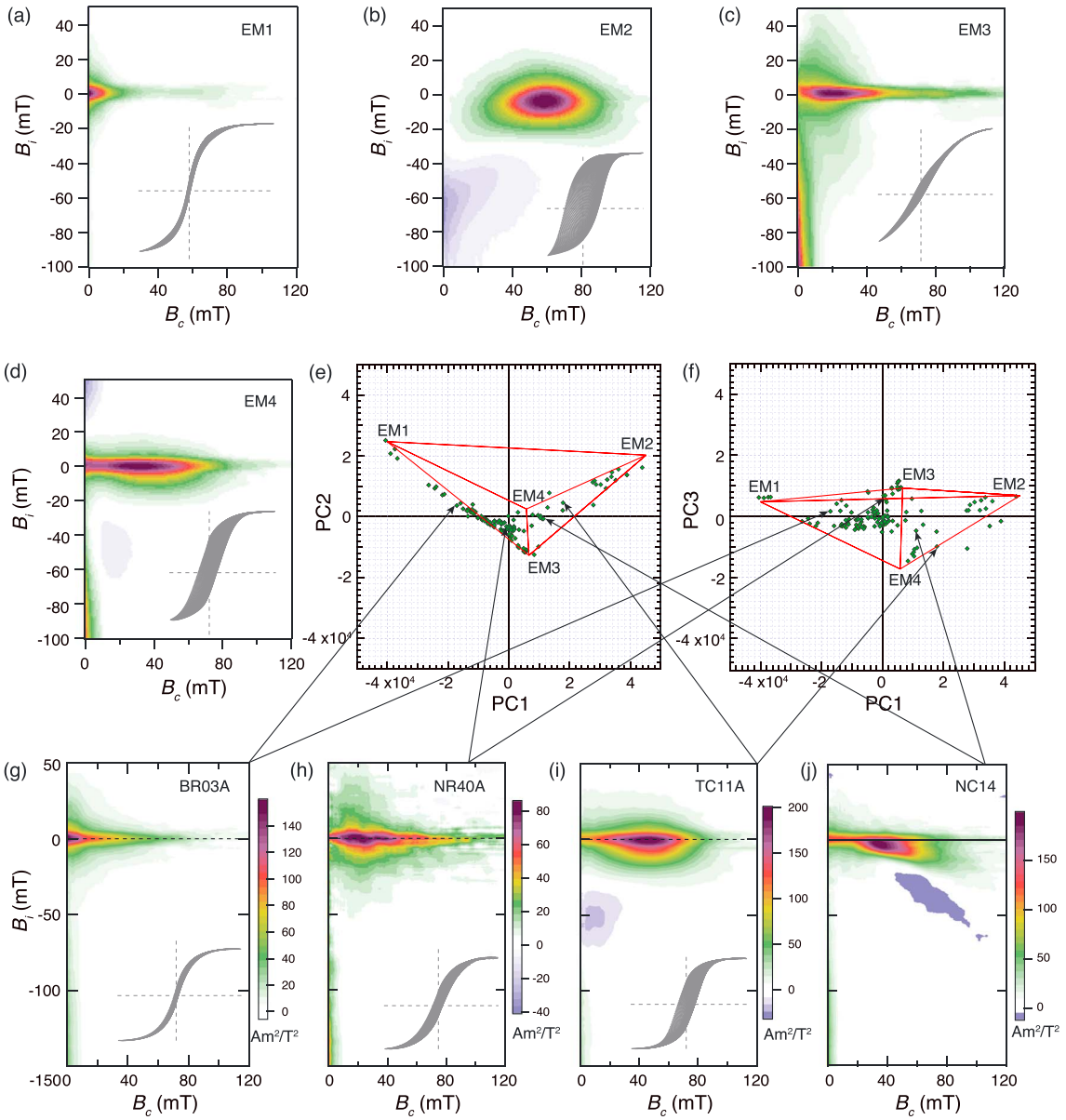

Figure 7. FORC unmixing results for sulfidic diagenetic environments in tectonically uplifted Neogene marine sediments from eastern New Zealand (Rowan & Roberts, 2006). Four EMs are identified, where (a) EM1 is a coarse detrital iron oxide component and (b) EM2 is stable SD greigite with strong magnetostatic interactions. EM3 and EM4 link the other two components, where both have a strong SP signal, but (c) EM3 contains a SD/vortex state detrital fraction, and (d) EM4 comprises a less strongly interacting SP/SD greigite component. (e and f) Visualizations of a tetrahedral mixing space (129 samples) for (e) PC1-PC2 and (f) PC1-PC3. (g–j) Representative FORC diagrams for measured samples that represent mixtures between (g) EM1 and EM3; (h) EM1, EM3, and EM4; (i) EM2, EM3, and EM4; and (j) EM2, EM3, and EM4. VARIFORC parameters (see Egli, 2013) for smoothing of the PCA solution are $s_{c,0} = 8$, $s_{c,1} = 10$, $s_{b,0} = 7$, $s_{b,1} = 10$, and $\lambda_c = \lambda_b = 0.1$. The maximum applied fields for FORC measurements were either 500 or 1,000 mT, which is sufficient to saturate magnetically the low-coercivity minerals in the studied samples.

and various EMs evidently consist of such mixtures (e.g., EM1 in Figure 3; EM3 in Figure 7). Nevertheless, the domain states represented by each EM are understandable in terms of the framework provided in Figure 2. In addition to recognizing domain states, FORC results can reveal features related to the type of magnetic anisotropy that controls the magnetization in different minerals. For example, SD particles with uniaxial anisotropy always have a negative peak along the B_i axis (Muxworthy et al., 2004; Newell, 2005). Harrison and Lascu (2014) demonstrated that FORC distributions for SD particles with cubic anisotropy also have such a peak (feature 1 in Figure 5f) as well as an additional negative peak below the main positive peak with elongation at −45° (feature 2 in Figure 5f). Such negative elongated peaks can be obscured by

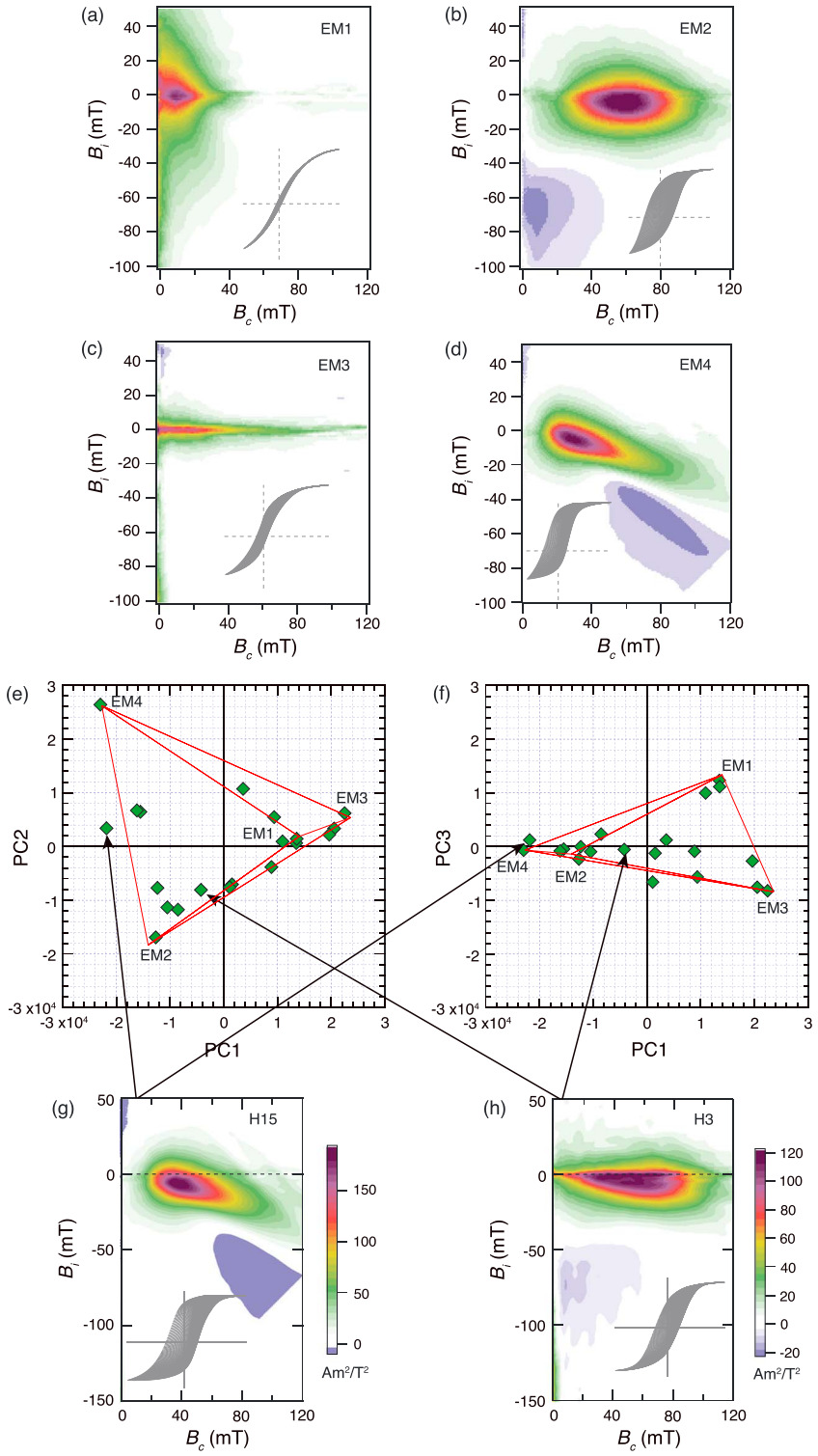

Figure 8. FORC unmixing results for sulfidic and methanic diagenetic environments in sediments with active methane venting from Hydrate Ridge, Cascadia margin, offshore of Oregon, USA (Larrasoaña et al., 2007). Four EMs are identified, where (a) EM1 is a coarse detrital iron oxide component (in turbidite samples), (b) EM2 is stable SD greigite with strong magnetostatic interactions, (c) EM3 is an authigenic SP-SD component, and (d) EM4 is magnetostatically interacting pyrrhotite, where the negative region at −45° is indicative of multiaxial anisotropy (see Harrison and Lascu, 2014). Visualizations of tetrahedral mixing (20 samples) for (e) PC1-PC2 and (f) PC1-PC3. Representative FORC diagrams for measured samples that represent mixtures between (g) EM2 and EM4 and (h) EM2 and EM3. The mixing space is well defined by measured samples that represent each EM, so contours are not shown to indicate the space for physically realistic FORCs. VARIFORC parameters (see Egli, 2013) for smoothing of the PCA solution are $s_{c,0} = 5$, $s_{c,1} = 7$, $s_{b,0} = 4$, $s_{b,1} = 7$, and $\lambda_c = \lambda_b = 0.1$. The maximum applied field for FORC measurements was 500 mT, which is sufficient to saturate magnetically the low-coercivity minerals in the studied samples.

various features, including mixtures of domain states and strong magnetostatic interactions (Harrison & Lascu, 2014), but when they are present, they indicate the presence of magnetic particles with multiaxial rather than uniaxial anisotropy. The presence of negative peaks such as feature 2 in Figure 5f in greigite-bearing samples and EMs as documented here (Figure 5a) confirms that greigite has cubic magnetocrystalline anisotropy (Roberts, 1995; Roberts et al., 2011). This type of negative peak is also seen systematically in FORC diagrams for authigenic pyrrhotite (Figures 8d and 8g) that forms in methanic environments (e.g., Horng, 2018; Kars & Kodama, 2015a, 2015b; Larrasoaña et al., 2007; Roberts et al., 2010; Weaver et al., 2002). This is due to triaxial anisotropy in the basal plane of pyrrhotite crystals (Martín-Hernández et al., 2008). Such features provide diagnostic information about magnetocrystalline anisotropy type, which is relevant to magnetic mineral identification, in addition to providing information about domain state. Importantly, even though pyrrhotite and greigite give rise to negative peaks with elongation at −45°, FORC distributions for authigenic pyrrhotite typically have lower coercivity and negative slopes (Figures 6a, 6g, 7j, 8d, and 8g) than those for greigite (Figures 5a and 5f).

5.2. Diagenetic Processes and Interpretation of FORC Unmixing Results

The EMs identified in the above examples from well-studied settings provide a consistent and systematic view of the magnetic properties associated with different diagenetic zones and of well-documented diagenetic processes in these reducing sediments. Linking these characteristic FORC results to diagenetic processes (Figure 9) should assist future studies of sediments that have undergone similar magnetic mineral diagenesis. Below we outline the main magnetic properties and diagenetic processes that affect magnetic minerals in the oxic to ferruginous, sulfidic, and methanic zones (Figure 9), respectively.

5.2.1. Oxic to Ferruginous Diagenesis

Surficial seafloor, lake bed, or river bed sediments are likely to contain primary magnetic mineral assemblages with relatively little diagenetic modification, especially if bottom waters are oxic. Compared to the pervasive diagenetic modification of magnetic minerals that occurs in the sulfidic and methanic zones, modification of magnetic minerals is relatively minor in the oxic, nitrogenous, and manganous zones and starts to become more significant in the ferruginous zone (Roberts, 2015). Cores CD143-55705 and LC13-81-G138 lack pore water chemistry data, but a diagenetic zonation can be developed by combining FORC results with the scanning electron microscope (SEM) observations of Rowan et al. (2009) and the SEM and transmission electron microscope (TEM) observations of Chang, Heslop, et al. (2016) because observed biogenic and authigenic minerals can be linked to the biogeochemistry of sedimentary environments (Berner, 1981).

Addition of biogenic magnetite to primary detrital magnetic mineral assemblages contributes significantly to the magnetic properties of surface sediments in cores CD143-55705 and LC13-81-G138. Magnetotactic bacteria generally biomineralize magnetite at the base of the nitrogenous zone (Figure 9), which may occur in the water column or uppermost sediment column, where iron is bioavailable due to upward diffusion of dissolved Fe^{2+} from the underlying ferruginous zone (Roberts, 2015). Contributions from the inorganic postmortem remains of magnetotactic bacteria are evident from a central ridge signature (Figures 3d and 4d) in FORC diagrams (Egli et al., 2010; Roberts et al., 2012) from the uppermost sediments in cores CD143-55705 and LC13-81-G138 (Figure 9). TEM observations (Chang, Heslop, et al., 2016) demonstrate the presence of fossil magnetosomes in these surficial sediments and confirm our interpretation of the central ridge FORC signature. Fine-grained bacterial magnetite is highly reactive under reducing conditions, and EM1 is depleted progressively with depth in both cores (Figures 3j and 4i). This loss of the finest magnetite population can occur in association with iron reduction in the ferruginous diagenetic zone or with sulfate reduction in the sulfidic zone and enhances the contribution of a coarser EM2 vortex state/MD component (Figures 3j and 4i). Chang, Heslop, et al. (2016) demonstrated that detrital and biogenic magnetite have different Verwey transition temperatures and used this to demonstrate that biogenic magnetite persists to depths of ~4.6 m in core CD143-55705 at which point the IRM is depleted to low values. From SEM observations, Rowan et al. (2009) documented minor sedimentary pyrite at depths of 0.1 m below the top of core CD143-55705, which indicates that sulfidic conditions were established close to the sediment-water interface (cf. Berner, 1981) and that the overlying diagenetic zones must be extremely thin. Both studied sediment cores occur in regions with an oceanic oxygen minimum zone but were both taken from below the modern oxygen minimum zone (Levin, 2003). Bottom waters in these settings are oxic, and the rapid progression to sulfidic conditions at shallow depths is likely due to high organic carbon inputs and microbial respiration of

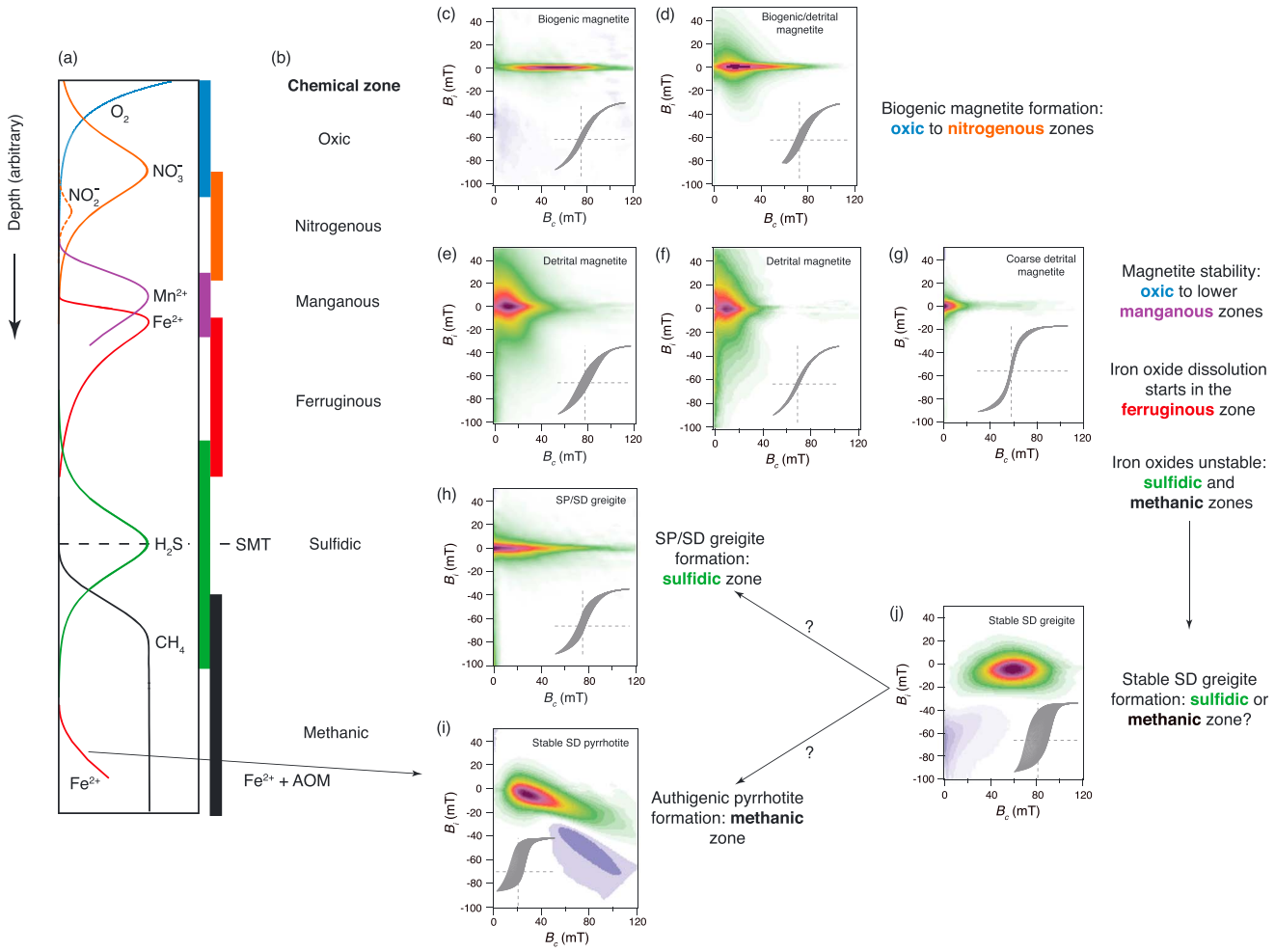

Figure 9. Illustration of typical FORC diagrams encountered in different diagenetic environments. (a) Schematic pore water profile for progressive steady state diagenesis and (b) chemical zones from Figure 1. FORC diagrams that are typical of (c) biogenic magnetite and (d) biogenic magnetite and a fine detrital magnetite fraction are encountered typically in oxic to ferruginous environments. Biogenic magnetite ceases to be stable in ferruginous environments. (e–g) Variable FORC diagrams are typically observed for detrital magnetic mineral assemblages containing magnetite with variable grain sizes, where coarse magnetite remains stable in oxic to manganous zones and starts to dissolve in the ferruginous zone. Iron oxides are unstable in the sulfidic and methanic zones and are unlikely to survive (unless they occur as inclusions within silicate particles; e.g., Chang, Bolton, et al., 2016; Chang, Roberts, et al., 2016). At the SMT, dissolved sulfide reacts with any available Fe^{2+} to form (h) SP/SD greigite. (i) If Fe^{2+} is available in the methanic zone, stable SD authigenic pyrrhotite can grow. (j) Stable SD greigite is encountered widely in reducing diagenetic environments, but it has not been linked definitively to the SMT and it could form deeper within the sediment column where Fe^{2+} is available and AOM creates a source of H_2S to enable greigite formation. The location of stable SD greigite formation is therefore indicated with question marks. Note that while the FORC diagrams presented in this figure are typical of the environments in question, they are not necessarily unique to these environments.

this organic matter near the sediment-water interface. Oxic to ferruginous diagenetic zones in the studied cores are likely to have been present because upward diffusion of bioavailable Fe^{2+} from the ferruginous zone is likely to have been used by magnetotactic bacteria to biomineralize magnetite at the base of the nitrogenous zone. Nevertheless, these zones would have been thin considering the shallow depths at which pyrite is present in these sediments. All further magnetic mineral diagenesis in these cores will have occurred under sulfidic or methanic conditions, as discussed below.

5.2.2. Sulfidic Diagenesis

Dissolution of magnetite and hematite becomes ubiquitous in sulfidic sediments (Canfield & Berner, 1987). Dissolved Fe^{2+} released from detrital and biogenic iron-bearing minerals reacts with dissolved H_2S, which is a by-product of sulfate reduction, to form sedimentary iron sulfides, particularly pyrite (Berner, 1984). Dissolution of detrital magnetite and hematite during sulfidic diagenesis, and replacement by paramagnetic pyrite, which does not carry a permanent magnetization, progressively destroys the primary

paleomagnetic record. Hematite is less reactive than magnetite in reducing environments (Emiroglu et al., 2004; Garming et al., 2005; Kawamura et al., 2007; Korff et al., 2016; Liu et al., 2004; Rey et al., 2005; Roberts, 2015; Robinson et al., 2000; Rowan et al., 2009; Yamazaki et al., 2003), but it will also undergo progressive dissolution with depth. We do not discuss the fate of hematite further in this context because it is less visible in FORC diagrams than magnetite (see section 2.1 above). Progressive loss of detrital and biogenic magnetic minerals via dissolution and pyrite formation is evident in the upper parts of cores CD143-55705 and LC13-81-G138 (Figures 3j and 4i). The presence of pyrite at shallow depths in core CD143-55705 (Rowan et al., 2009; Chang, Heslop, et al., 2016) indicates that sulfidic conditions existed just below the sediment-water interface, which raises the question of why surficial IRM values decrease to low values down-core in two steps rather than one (Figure 3j) in core CD143-55705. The lower IRM peak is depleted in biogenic magnetite (EM1) and is enriched in the coarser vortex state/MD detrital component (EM2). In core CD143-55705, there is a local increase in the diagenetic SP/SD greigite component (EM3) in the minimum between IRM peaks. EM3 is then the only component below the lower IRM peak. These features indicate that the base of the upper IRM peak represents the modern sulfate-methane transition (SMT; Figure 9). The base of the lower IRM peak likely represents a former SMT position, which migrated upward with a change in sedimentary conditions to leave a relict coarse detrital component (EM2) between the old and new sulfidic dissolution fronts (Riedinger et al., 2005; Rowan et al., 2009). Even though biogenic magnetite is fine-grained and reactive to dissolved sulfide, low-temperature magnetic measurements indicate that minor magnetofossil concentrations remain in core CD143-55705 to depths of ~4.6 m in correspondence with the former SMT position (Chang, Heslop, et al., 2016).

Once detrital and biogenic magnetic components have been dissolved by sulfidic diagenesis, the only magnetic minerals that are likely to remain are authigenic minerals that form in reducing environments, relict minerals that are unreactive or slowly reactive to sulfide, such as chromite (Hounslow, 1996), titanohematites (Franke et al., 2007; Garming et al., 2007), or iron oxide inclusions within silicate minerals that are protected from sulfidization by their silicate hosts (Roberts, 2015; Chang, Bolton, et al., 2016; Chang, Roberts, et al., 2016). The only component detected with FORC unmixing below the former SMT position at ~4.6 m in core CD143-55705 (Figure 3i) is an authigenic SP/SD greigite component (EM3). This component is fine-grained, weak, and lacks strong magnetostatic interactions. It is possible that the magnetically noninteracting SD part of EM3 (Figures 3i and 4f) is a central ridge signature (Egli et al., 2010) associated with greigite-bearing magnetotactic bacteria. Identification of ancient magnetite magnetofossils has expanded greatly with joint use of FORC diagrams and TEM observations (e.g., Roberts et al., 2012; Yamazaki, 2008, 2009; Yamazaki & Ikehara, 2012). Roberts (2015) suggested that greigite magnetofossils should be more abundant in the geological record than magnetite magnetofossils, particularly if they are gradient organisms (Bazylinski & Frankel, 2004) that live near the so-called oxic-anoxic interface (i.e., nitrogenous to ferruginous boundary in Figure 1), because magnetite dissolves when buried into the sulfidic diagenetic zone, whereas greigite remains stable. Widespread greigite magnetofossil occurrence remains undemonstrated and is an important research avenue. The link between central ridge FORC signatures and greigite magnetofossils is established (Chang et al., 2014; Chen et al., 2014; Reinholdsson et al., 2013), but the challenge will be to provide convincing evidence from TEM observations of greigite magnetosomes, which do not have the ideal crystal morphology or chain arrangement of magnetite magnetosomes (Farina et al., 1990; Kasama et al., 2006; Mann et al., 1990; Pósfai et al., 1998a, 1998b).

Greigite formation has been documented in modern continental margin marine sediments at depths of several meters to tens of meters below the sediment-water interface (Fu et al., 2008; Jørgensen et al., 2004; Kasten et al., 1998; Larrasoaña et al., 2007; Liu et al., 2004; Neretin et al., 2004; Riedinger et al., 2005, 2014; Rowan et al., 2009). Strongly magnetized stable SD greigite with strong magnetostatic interactions that is typically associated with sulfidic diagenesis (EM2 in Figures 5–8) is not evident in the relatively short sediment cores discussed here. There is therefore a disconnect in our understanding of early diagenesis and the point at which the strongly interacting stable SD greigite grows. It has been assumed that initial SP/SD greigite assemblages (EM3 in Figures 3–8) continue to grow through the stable SD blocking volume with progressive sulfidization at depth to transform into such assemblages (Rowan & Roberts, 2006; Rowan et al., 2009), but marine sediment cores are usually not long enough to assess whether this progressive greigite formation mechanism is correct. Liu et al. (2016) documented strongly interacting stable SD greigite in discrete sediment layers from a long sediment core from the South Yellow Sea starting from depths of ~6 m below the

sediment-water interface. However, this shallow water setting has been subjected to major nonsteady state diagenetic changes associated with large-amplitude Quaternary sea level variations and lack of a pore water profile makes it difficult to assess the diagenetic environment in which this greigite formed. Stable SD greigite has been documented extensively within sediments in methanic environments in association with AOM (Enkin et al., 2007; Horng & Chen, 2006; Housen & Musgrave, 1996; Kars & Kodama, 2015a, 2015b; Larrasoaña et al., 2007; Musgrave et al., 2006; Shi et al., 2017), so the possibility of greigite formation in either the sulfidic or methanic zones should be considered (Figure 9). The depth of this greigite formation has important consequences for the timing of sedimentary paleomagnetic signal acquisition. Rowan et al. (2009) estimated from widely distributed sediment cores that the onset of early greigite formation at the SMT (with properties like EM3) starts from 0.6 to >220 kyr after deposition depending on the sedimentation rate, with SD greigite formation in underlying sediments occurring over periods of ≥1 to ≥160 kyr. Later formation in the methanic zone can lead to remanence acquisition delays of a few kyr to Myr (Larrasoaña et al., 2007), including complete remagnetization (Roberts & Weaver, 2005). Assessing recording delays associated with greigite growth is a key issue in magnetic studies of diagenetically reduced sediments.

5.2.3. Methanic Diagenesis

In the methanic diagenetic zone, AOM is the most important known process that affects magnetic mineral assemblages (Roberts, 2015). Sulfate reduction via AOM consumes pore water methane and sulfate to depletion at the SMT (Figure 1) and provides a secondary, relatively mobile, source of H_2S (Devol & Ahmed, 1981; Jørgensen & Kasten, 2006; Kasten & Jørgensen, 2000; Murray et al., 1978; Niewöhner et al., 1998) that can cause both reductive dissolution of detrital iron oxides and formation of secondary ferrimagnetic iron sulfides. If the SMT occurs at shallow depths, as in the examples shown in Figures 3 and 4, early diagenetic greigite growth will result in relatively short delays in paleomagnetic signal acquisition. If Fe^{2+} and H_2S are available at greater depths (Figure 9), however, greigite can form at any time during diagenesis (Roberts & Weaver, 2005). Fe^{2+} concentrations can increase within the methanic zone due to coupling of AOM to Fe and Mn reduction (Beal et al., 2009; Egger et al., 2015; Riedinger et al., 2014; Segarra et al., 2013; Sivan et al., 2011). While dissolved sulfide production is expected at the SMT during steady state diagenesis (Figure 1), methane is often mobilized through fracture and fault networks in tectonically active settings. AOM of this mobile methane can release H_2S that will react with any available Fe^{2+} to cause magnetic iron sulfide formation at any time during diagenesis (Figure 9), which makes AOM an important process in magnetic mineral diagenesis. Greigite is known to occur in methane-rich sediments or in methane hydrates (e.g., Enkin et al., 2007; Horng & Chen, 2006; Housen & Musgrave, 1996; Musgrave et al., 2006), while greigite and pyrrhotite also form in association with methane diffusion (Figures 5, 8, and 9; Larrasoaña et al., 2007).

Potential greigite formation during both sulfidic and methanic diagenesis (Figure 9) raises questions about the diagenetic zone in which the stable SD greigite formed in the case studies illustrated in Figures 5–8. The presence of greigite in methanic environments is generally associated with its formation during earlier sulfidic diagenesis, but this is not necessarily the case. The common occurrence of remagnetizations in greigite-bearing sediments of eastern North Island, New Zealand, led Rowan and Roberts (2008) to suggest that late greigite formation was associated with deeper diagenetic processes such as gas hydrate formation and AOM. Likewise, van Dongen et al. (2007) demonstrated from organic geochemical evidence that AOM occurred within greigite-bearing nodules. Nevertheless, assumed linkages between greigite formation and sulfidic environments have not been questioned widely. In addition to greigite, pyrrhotite has been documented widely in association with methane hydrates (Enkin et al., 2007; Horng & Chen, 2006; Housen & Musgrave, 1996; Musgrave et al., 2006; Rudmin et al., 2018) and in tectonically fractured areas that support active methane diffusion or venting (Larrasoaña et al., 2007), which suggests that authigenic pyrrhotite is an indicator of methanic environments (Figure 9). The authigenic pyrrhotite that forms in methanic environments is magnetic so it has been assumed widely to be monoclinic pyrrhotite (e.g., Kars & Kodama, 2015a; Larrasoaña et al., 2007; Roberts, 2015; Weaver et al., 2002). Horng (2018) and Horng and Roberts (2018) demonstrated recently that authigenic pyrrhotite in methanic sediments has an unambiguous hexagonal rather than monoclinic crystal structure. Hexagonal pyrrhotite is expected to be antiferromagnetic, so further work is needed to understand and explain its magnetic structure.

The above observations raise the question of whether sulfidic and methanic diagenetic environments can be distinguished from each other from the magnetic properties of magnetic mineral assemblages. Characteristic kidney-shaped FORC distributions with negative slopes for SD pyrrhotite and a negative region also with

negative slope (Horng, 2018; Kars & Kodama, 2015a, 2015b; Larrasoaña et al., 2007; Roberts et al., 2010; Weaver et al., 2002; Wehland et al., 2005) suggest that pyrrhotite can be identified readily from FORC distributions (Figures 8d and 8g). This negative region is sometimes not evident because of the scaling of FORC diagrams, but it can be made more visible through manual adjustment of the color scale. Nevertheless, the negative slope of the positive part of FORC distributions for pyrrhotite-bearing samples is distinct from FORC distributions for greigite-bearing samples. Additionally, the peak coercivity of FORC distributions for our SD greigite-bearing samples is ~60–70 mT, while it is ~20–40 mT for our pyrrhotite-bearing samples. Based on these observations, we suggest that the Crostolo River sediments contain previously unidentified pyrrhotite (Figures 6a, 6g, and 6h). In contrast, Tric et al. (1991) argued that the Crostolo Rover sediments contain a detailed Upper Olduvai polarity transition record associated with greigite that grew during earliest burial. Roberts et al. (2005) demonstrated from detailed SEM observations that different generations of greigite formed in these sediments, but they could not constrain the timescales involved and concluded that it was relatively early. Our new evidence indicates that these sediments record magnetic signatures associated with both sulfidic and methanic stages, which illustrates the potential difficulties in discriminating in which of these two stages greigite formed. Magnetic signatures due to pyrrhotite have not been detected previously in the Crostolo River sediments, which provide new information about the diagenetic history of these sediments. It is important to note that pyrrhotite is not always identified in association with methane hydrates (e.g., Shi et al., 2017). Also, even though remagnetization of sediments from eastern North Island, New Zealand, has been attributed to tectonically driven methane migration (Rowan & Roberts, 2008), no pyrrhotite is evident in FORC diagrams from these sediments (Figure 7). However, pyrrhotite FORC signatures are evident in four samples from the NC locality (Figure 7j) in northeastern South Island (Rowan & Roberts, 2006), which indicates that these sediments experienced methanic diagenesis. Overall, though, key markers for diagenetic processes of interest may not always be present. As ever, positive evidence is important and an absence of evidence provides neither confirmation nor disproof of a process.

6. Conclusions

FORC unmixing with PCA provides clear detection of magnetic properties associated with magnetic mineral diagenesis during early sediment burial. From our analysis of multiple data sets (FORC measurements for $>$240 samples), consistent magnetic components are identified from sediments that have undergone various stages of reductive diagenesis (Figure 9). Relatively unaltered magnetic assemblages in oxic to manganous diagenetic zones are rich in coarse detrital magnetic minerals and fine biogenic magnetite. These minerals dissolve progressively in ferruginous and sulfidic diagenetic environments and largely disappear when buried to the base of the sulfidic zone at the SMT. Below the SMT, authigenic phases dominate magnetic mineral assemblages. An initial weak and magnetostatically weakly interacting authigenic SP/SD greigite component is identified in all studied sulfidic and methanic settings, along with stable and strongly interacting SD greigite. An additional magnetostatically interacting pyrrhotite component is identified in methanic environments. Mixtures of the components are common in the respective environments; FORC unmixing enables quantification of the contributions of each component. Identification of FORC signatures for each component and association of their magnetic properties with the diagenetic processes to which they have been subjected provides information concerning sedimentary magnetic signatures that will enable researchers to grapple with relevant questions that arise when considering diagenesis and its effects on paleomagnetic and environmental signals.

Despite the clarity of our results concerning the magnetic mineral components that occur in reducing diagenetic environments, our work raises a key unresolved question. Greigite can form in both sulfidic and methanic diagenetic environments (Figure 9); in most cases where greigite has been identified, it remains unknown in which of these diagenetic zones greigite formed. Significant smoothing can affect paleomagnetic and environmental signal acquisition in both cases, but smoothing will be a more significant complication in deeper methanic environments. Determining the environment in which greigite formed is important for understanding magnetic signals associated with sedimentary reductive diagenetic processes. It is important to gain a better understanding in future studies of the extent to which stable SD greigite grows in sulfidic versus methanic diagenetic environments. It is also important to note that authigenic pyrrhotite forms in methanic environments, so it will usually record a delayed paleomagnetic signal.

Acknowledgments
This work was supported financially by the Australian Research Council through grant DP160100805, by the European Research Council under the European Union's Seventh Framework Programme (FP/2007–2013)/ERC grant agreement number 320750, and by the National Institute of Advanced Industrial Science and Technology, Ministry of Economy, Trade and Industry, Japan. We thank Luca Lanci and Tilo von Dobeneck for constructive reviews that improved this paper, Michael Walter for editorial handling, and Sue Wigley for organizing a writing week that enabled the first five authors of this paper to finalize the unmixing algorithm and prepare manuscripts for publication. The authors are in the process of creating a global FORC database to which the data presented in this paper will be added after publication.

References

Bazylinski, D. A., & Frankel, R. B. (2004). Magnetosome formation in prokaryotes. *Nature Reviews Microbiology*, *2*, 217–230.

Beal, E. J., House, C. H., & Orphan, V. J. (2009). Manganese- and iron-dependent marine methane oxidation. *Science*, *325*, 184–187.

Berner, R. A. (1981). A new geochemical classification of sedimentary environments. *Journal of Sedimentary Petrology*, *51*, 359–365.

Berner, R. A. (1984). Sedimentary pyrite formation: An update. *Geochimica et Cosmochimica Acta*, *48*, 605–615.

Bouilloux, A., Valet, J. P., Bassinot, F., Joron, J. L., Blanc-Valleron, M. M., Moreno, E., et al. (2013). Diagenetic modulation of the magnetic properties in sediments from the northern Indian Ocean. *Geochemistry, Geophysics, Geosystems*, *14*, 3779–3800. https://doi.org/10.1002/ggge.20234

Canfield, D. E., & Berner, R. A. (1987). Dissolution and pyritization of magnetite in anoxic marine sediments. *Geochimica et Cosmochimica Acta*, *51*, 645–659.

Canfield, D. E., & Thamdrup, B. (2009). Towards a consistent classification scheme for geochemical environments, or, why we wish the term 'suboxic' would go away. *Geobiology*, *7*, 385–392.

Carvallo, C., Roberts, A. P., Leonhardt, R., Laj, C., Kissel, C., Perrin, M., & Camps, P. (2006). Increasing the efficiency of paleointensity analyses by selection of samples using first-order reversal curve (FORC) diagrams. *Journal of Geophysical Research*, *111*, B12103. https://doi.org/10.1029/2005JB004126

Chang, L., Bolton, C. T., Dekkers, M. J., Hayashida, A., Heslop, D., Krijgsman, W., et al. (2016). Asian monsoon modulation of nonsteady state diagenesis in hemipelagic marine sediments offshore of Japan. *Geochemistry, Geophysics, Geosystems*, *17*, 4383–4398. https://doi.org/10.1002/2016GC006344

Chang, L., Heslop, D., Roberts, A. P., Rey, D., & Mohamed, K. J. (2016). Discrimination of biogenic and detrital magnetite through a double Verwey transition temperature. *Journal of Geophysical Research: Solid Earth*, *121*, 3–14. https://doi.org/10.1002/2015JB012485

Chang, L., Roberts, A. P., Heslop, D., Hayashida, A., Li, J. H., Zhao, X., et al. (2016). Widespread occurrence of silicate-hosted magnetic mineral inclusions in marine sediments and their contribution to paleomagnetic recording. *Journal of Geophysical Research: Solid Earth*, *121*, 8415–8431. https://doi.org/10.1002/2016JB013109

Chang, L., Vasiliev, I., van Baak, C., Krijgsman, W., Dekkers, M. J., Roberts, A. P., et al. (2014). Identification and environmental interpretation of diagenetic and biogenic greigite in sediments: A lesson from the Messinian Black Sea. *Geochemistry, Geophysics, Geosystems*, *15*, 3612–3627. https://doi.org/10.1002/2014GC005411

Channell, J. E. T., Harrison, R. J., Lascu, I., McCave, I. N., Hibbert, F. D., & Austin, W. E. N. (2016). Magnetic record of deglaciation using FORC-PCA, sortable-silt grain size, and magnetic excursion at 26 ka, from the Rockall Trough (NE Atlantic). *Geochemistry, Geophysics, Geosystems*, *17*, 1823–1841. https://doi.org/10.1002/2016GC006300

Channell, J. E. T., & Hawthorne, T. (1990). Progressive dissolution of titanomagnetites at ODP Site 653 (Tyrrhenian Sea). *Earth and Planetary Science Letters*, *96*, 469–480.

Chen, A. P., Berounsky, V. M., Chan, M. K., Blackford, M. G., Cady, C., Moskowitz, B. M., et al. (2014). Magnetic properties of uncultivated magnetotactic bacteria and their contribution to a stratified estuary iron cycle. *Nature Communications*, *5*, 4797. https://doi.org/10.1038/ncomms5797

Chen, L., Heslop, D., Roberts, A. P., Chang, L., Zhao, X., McGregor, H. V., et al. (2017). Remanence acquisition efficiency in biogenic and detrital magnetite and recording of geomagnetic paleointensity. *Geochemistry, Geophysics, Geosystems*, *18*, 1435–1450. https://doi.org/10.1002/2016GC006753

Devol, A. H., & Ahmed, S. I. (1981). Are high rates of sulphate reduction associated with anaerobic oxidation of methane? *Nature*, *291*, 407–408.

Dillon, M., & Bleil, U. (2006). Rock magnetic signatures in diagenetically altered sediments from the Niger deep-sea fan. *Journal of Geophysical Research*, *111*, B03105. https://doi.org/10.1029/2004JB003540

Egger, M., Rasigraf, O., Sapart, C. J., Jilbert, T., Jetten, M. S. M., Röckmann, T., et al. (2015). Iron-mediated anaerobic oxidation of methane in brackish coastal sediments. *Environmental Science and Technology*, *49*, 277–283.

Egli, R. (2004a). Characterization of individual rock magnetic components by analysis of remanence curves, 1. Unmixing natural sediments. *Studia Geophysica et Geodaetica*, *48*, 391–446.

Egli, R. (2004b). Characterization of individual rock magnetic components by analysis of remanence curves, 2. Fundamental properties of coercivity distributions. *Physics and Chemistry of the Earth*, *29*, 851–867.

Egli, R. (2004c). Characterization of individual rock magnetic components by analysis of remanence curves. 3. Bacterial magnetite and natural processes in lakes. *Physics and Chemistry of the Earth*, *29*, 869–884.

Egli, R. (2013). VARIFORC: An optimized protocol for calculating non-regular first-order reversal curve (FORC) diagrams. *Global and Planetary Change*, *110*, 302–320.

Egli, R., Chen, A. P., Winklhofer, M., Kodama, K. P., & Horng, C. S. (2010). Detection of noninteracting single domain particles using first-order reversal curve diagrams. *Geochemistry, Geophysics, Geosystems*, *11*, Q01Z11. https://doi.org/10.1029/2009GC002916

Emiroglu, S., Rey, D., & Petersen, N. (2004). Magnetic properties of sediment in the Ria de Arousa (Spain): Dissolution of iron oxides and formation of iron sulphides. *Physics and Chemistry of the Earth*, *29*, 947–959.

Enkin, R. J., Baker, J., Nourgaliev, D., Iassonov, P., & Hamilton, T. S. (2007). Magnetic hysteresis parameters and Day plot analysis to characterize diagenetic alteration in gas hydrate bearing sediments. *Journal of Geophysical Research*, *112*, B06S90. https://doi.org/10.1029/2006JB004638

Farina, M., Esquivel, D. M. S., & Lins de Barros, H. G. P. (1990). Magnetic iron-sulphur crystals from a magnetotactic microorganism. *Nature*, *343*, 256–258.

Florindo, F., Karner, D. B., Marra, F., Renne, P. R., Roberts, A. P., & Weaver, R. (2007). Radioisotopic age constraints for glacial terminations IX and VII from aggradational sections of the Tiber River delta in Rome, Italy. *Earth and Planetary Science Letters*, *256*, 61–80.

Franke, C., Pennock, G. M., Drury, M. R., Engelmann, R., Lattard, D., Garming, J. F. L., et al. (2007). Identification of magnetic Fe-Ti oxides in marine sediments by electron backscatter diffraction in scanning electron microscopy. *Geophysical Journal International*, *170*, 545–555.

Froelich, P. N., Klinkhammer, G. P., Bender, M. L., Luedtke, N. A., Heath, G. R., Cullen, D., et al. (1979). Early oxidation of organic matter in pelagic sediments of the eastern equatorial Atlantic: Suboxic diagenesis. *Geochimica et Cosmochimica Acta*, *43*, 1075–1090.

Fu, Y., von Dobeneck, T., Franke, C., Heslop, D., & Kasten, S. (2008). Rock magnetic identification and geochemical process models of greigite formation in Quaternary marine sediments from the Gulf of Mexico (IODP Hole U1319A). *Earth and Planetary Science Letters*, *275*, 233–245.

Garming, J. F. L., Bleil, U., & Riedinger, N. (2005). Alteration of magnetic mineralogy at the sulfate–methane transition: Analysis of sediments from the Argentine continental slope. *Physics of the Earth and Planetary Interiors*, *151*, 290–308.

Garming, J. F. L., von Dobeneck, T., Franke, C., & Bleil, U. (2007). Low-temperature partial magnetic self-reversal in marine sediments by magnetostatic interaction of titanomagnetite and titanohematite intergrowths. *Geophysical Journal International*, *170*, 1067–1075.
Harrison, R. J., & Feinberg, J. M. (2008). FORCinel: An improved algorithm for calculating first-order reversal curve distributions using locally weighted regression smoothing. *Geochemistry, Geophysics, Geosystems*, *9*, Q05016. https://doi.org/10.1029/2008GC001987
Harrison, R. J., & Lascu, I. (2014). FORCulator: A micromagnetic tool for simulating first-order reversal curve diagrams. *Geochemistry, Geophysics, Geosystems*, *15*, 4671–4691. https://doi.org/10.1002/2014GC005582
Harrison, R. J., Muraszko, J., Heslop, D., Lascu, I., Muxworthy, A. R., & Roberts, A. P. (2018). An improved algorithm for unmixing first-order reversal curve diagrams using principal component analysis. *Geochemistry, Geophysics, Geosystems*, *19*. https://doi.org/10.1029/2018GC007511
Heslop, D. (2015). Numerical strategies for magnetic mineral unmixing. *Earth-Science Reviews*, *150*, 256–284.
Heslop, D., Dekkers, M. J., Kruiver, P. P., & van Oorschot, I. H. M. (2002). Analysis of isothermal remanent magnetization acquisition curves using the expectation-maximization algorithm. *Geophysical Journal International*, *148*, 58–64.
Heslop, D., & Dillon, M. (2007). Unmixing magnetic remanence curves without *a priori* knowledge. *Geophysical Journal International*, *170*, 556–566.
Heslop, D., Roberts, A. P., & Chang, L. (2014). Characterizing magnetofossils from first-order reversal curve (FORC) central ridge signatures. *Geochemistry, Geophysics, Geosystems*, *15*, 2170–2179. https://doi.org/10.1002/2014GC005291
Horng, C. S. (2018). Unusual magnetic properties of sedimentary pyrrhotite in methane seepage sediments: Comparison with metamorphic pyrrhotite and sedimentary greigite. *Journal of Geophysical Research: Solid Earth*, *123*. https://doi.org/10.1002/2017JB015262
Horng, C. S., & Chen, K. H. (2006). Complicated magnetic mineral assemblages in marine sediments offshore southwestern Taiwan: Possible influences of methane flux on the early diagenetic processes. *Terrestrial, Atmospheric and Oceanic Sciences*, *17*, 1009–1026.
Horng, C. S., & Roberts, A. P. (2018). The low-temperature Besnus magnetic transition: Signals due to monoclinic and hexagonal pyrrhotite. *Geochemistry, Geophysics, Geosystems*, *19*. https://doi.org/10.1002/2017GC007394
Hounslow, M. W. (1996). Ferrimagnetic Cr and Mn spinels in sediments: Residual magnetic minerals after diagenetic dissolution. *Geophysical Research Letters*, *23*, 2823–2826. https://doi.org/10.1029/96GL01327
Housen, B. A., & Musgrave, R. J. (1996). Rock-magnetic signature of gas hydrates in accretionary prism sediments. *Earth and Planetary Science Letters*, *139*, 509–519.
Jørgensen, B. B., Böttcher, M. E., Lüschen, H., Neretin, L. N., & Volkov, I. I. (2004). Anaerobic methane oxidation and a deep H_2S sink generate isotopically heavy sulfides in Black Sea sediments. *Geochimica et Cosmochimica Acta*, *68*, 2095–2118.
Jørgensen, B. B., & Kasten, S. (2006). Sulfur cycling and methane oxidation. In H. D. Schulz & M. Zabel (Eds.), *Marine Geochemistry* (pp. 271–309). Berlin: Springer.
Karlin, R. (1990a). Magnetite diagenesis in marine sediments from the Oregon continental margin. *Journal of Geophysical Research*, *95*, 4405–4419. https://doi.org/10.1029/JB095iB04p04405
Karlin, R. (1990b). Magnetic mineral diagenesis in suboxic sediments at Bettis site W-N, NE Pacific Ocean. *Journal of Geophysical Research*, *95*, 4421–4436. https://doi.org/10.1029/JB095iB04p04421
Karlin, R., & Levi, S. (1983). Diagenesis of magnetic minerals in Recent haemipelagic sediments. *Nature*, *303*, 327–330.
Karlin, R., & Levi, S. (1985). Geochemical and sedimentological control of the magnetic properties of hemipelagic sediments. *Journal of Geophysical Research*, *90*, 10,373–10,392. https://doi.org/10.1029/JB090iB12p10373
Kars, M., & Kodama, K. (2015a). Authigenesis of magnetic minerals in gas hydrate-bearing sediments in the Nankai Trough, offshore Japan. *Geochemistry, Geophysics, Geosystems*, *16*, 947–961. https://doi.org/10.1002/2014GC005614
Kars, M., & Kodama, K. (2015b). Rock magnetic characterization of ferrimagnetic iron sulfides in gas hydrate-bearing marine sediments at Site C0008, Nankai Trough, Pacific Ocean, off-coast Japan. *Earth, Planets and Space*, *67*, 118. https://doi.org/10.1186/s40623-015-0287-y
Kasama, T., Pósfai, M., Chong, R. K. K., Finlayson, A. P., Buseck, P. R., Frankel, R. B., & Dunin-Borkowski, R. E. (2006). Magnetic properties, microstructure, composition, and morphology of greigite nanocrystals in magnetotactic bacteria from electron holography and tomography. *American Mineralogist*, *91*, 1216–1229.
Kasten, S., Freudenthal, T., Gingele, F. X., & Schulz, H. D. (1998). Simultaneous formation of iron-rich layers at different redox boundaries in sediments of the Amazon deep-sea fan. *Geochimica et Cosmochimica Acta*, *62*, 2253–2264.
Kasten, S., & Jørgensen, B. B. (2000). Sulfate reduction in marine sediments. In H. D. Schulz & M. Zabel (Eds.), *Marine Geochemistry* (pp. 263–281). Berlin: Springer.
Kawamura, N., Oda, H., Ikehara, K., Yamazaki, T., Shioi, K., Taga, S., et al. (2007). Diagenetic effect on magnetic properties of marine core sediments from the southern Okhotsk Sea. *Earth, Planets and Space*, *59*, 83–93.
Korff, L., von Dobeneck, T., Frederichs, T., Kasten, S., Kuhn, G., Gersonde, R., & Diekmann, B. (2016). Cyclic magnetite dissolution in Pleistocene sediments of the abyssal Northwest Pacific Ocean: Evidence for glacial oxygen depletion and carbon trapping. *Paleoceanography*, *31*, 600–624. https://doi.org/10.1002/2015PA002882
Kruiver, P. P., Dekkers, M. J., & Heslop, D. (2001). Quantification of magnetic coercivity components by the analysis of acquisition curves of isothermal remanent magnetization. *Earth and Planetary Science Letters*, *189*, 269–276.
Lagroix, F., & Guyodo, Y. (2017). A new tool for separating the magnetic mineralogy of complex mineral assemblages from low temperature magnetic behavior. *Frontiers in Earth Science*, *5*, 61. https://doi.org/10.3389/feart.2017.00061
Larrasoaña, J. C., Roberts, A. P., Musgrave, R. J., Gràcia, E., Piñero, E., Vega, M., & Martínez-Ruiz, F. (2007). Diagenetic formation of greigite and pyrrhotite in marine sedimentary systems containing gas hydrates. *Earth and Planetary Science Letters*, *261*, 350–366.
Lascu, I., Harrison, R. J., Li, Y. T., Muraszko, J. R., Channell, J. E. T., Piotrowski, A. M., & Hodell, D. A. (2015). Magnetic unmixing of first-order reversal curve diagrams using principal component analysis. *Geochemistry, Geophysics, Geosystems*, *16*, 2900–2915. https://doi.org/10.1002/2015GC005909
Leslie, B. W., Hammond, D. E., Berelson, W. M., & Lund, S. P. (1990). Diagenesis in anoxic sediments from the California continental borderland and its influence on iron, sulfur, and magnetite behavior. *Journal of Geophysical Research*, *95*, 4453–4470. https://doi.org/10.1029/JB095iB04p04453
Leslie, B. W., Lund, S. P., & Hammond, D. E. (1990). Rock magnetic evidence for the dissolution and authigenic growth of magnetic minerals within anoxic marine sediments of the California continental borderland. *Journal of Geophysical Research*, *95*, 4437–4452. https://doi.org/10.1029/JB095iB04p04437
Levin, L. A. (2003). In R. N. Gibson & R. J. A. Atkinson (Eds.), *Oxygen minimum zone benthos: Adaptation and community response to hypoxia. Oceanography and Marine Biology: An Annual Review* (Vol. 41, pp. 1–45). London: CRC Press (Taylor & Francis Group).

Liu, J., Zhu, R. X., Roberts, A. P., Li, S. Q., & Chang, J. H. (2004). High-resolution analysis of early diagenetic effects on magnetic minerals in post-middle-Holocene continental shelf sediments from the Korea Strait. *Journal of Geophysical Research*, *109*, B03103. https://doi.org/10.1029/2003JB002813

Liu, J. X., Liu, Q. S., Zhang, X. H., Liu, J., Wu, Z. Q., Mei, X., et al. (2016). Magnetostratigraphy of a long Quaternary sediment core in the South Yellow Sea. *Quaternary Science Reviews*, *144*, 1–15.

Mann, S., Sparks, N. H. C., Frankel, R. B., Bazylinski, D. A., & Jannasch, H. W. (1990). Biomineralization of ferrimagnetic greigite (Fe_3S_4) and iron pyrite (FeS_2) in a magnetotactic bacterium. *Nature*, *343*, 258–261.

Martín-Hernández, F., Dekkers, M. J., Bominaar-Silkens, I. M. A., & Maan, J. C. (2008). Magnetic anisotropy behaviour of pyrrhotite as determined by low- and high-field experiments. *Geophysical Journal International*, *174*, 42–54.

Mohamed, K. J., Rey, D., Rubio, B., Dekkers, M. J., Roberts, A. P., & Vilas, F. (2011). Onshore-offshore gradient in reductive early diagenesis in coastal marine sediments of the Ria de Vigo, Northwest Iberian Peninsula. *Continental Shelf Research*, *31*, 433–447.

Murray, J. W., Grundmanis, V., Smethie, J., & William, M. (1978). Interstitial water chemistry in the sediments of Saanich Inlet. *Geochimica et Cosmochimica Acta*, *42*, 1011–1026.

Musgrave, R. J., Bangs, N. K., Larrasoaña, J. C., Gràcia, E., Hollamby, J. A., & Vega, M. E. (2006). Rise of the base of the gas hydrate zone since the last glacial recorded by rock magnetism. *Geology*, *34*, 117–120.

Muxworthy, A. R., & Dunlop, D. J. (2002). First-order reversal curve (FORC) diagrams for pseudo-single-domain magnetites at high temperature. *Earth and Planetary Science Letters*, *203*, 369–382.

Muxworthy, A. R., Heslop, D., & Williams, W. (2004). Influence of magnetostatic interactions on first-order-reversal-curve (FORC) diagrams: A micromagnetic approach. *Geophysical Journal International*, *158*, 888–897.

Muxworthy, A. R., King, J. G., & Heslop, D. (2005). Assessing the ability of first-order reversal curve (FORC) diagrams to unravel complex magnetic signals. *Journal of Geophysical Research*, *110*, B01105. https://doi.org/10.1029/2004JB003195

Neretin, L. N., Böttcher, M. E., Jørgensen, B. B., Volkov, I. I., Lüschen, H., & Hilgenfeldt, K. (2004). Pyritization processes and greigite formation in the advancing sulfidization front in the Upper Pleistocene sediments of the Black Sea. *Geochimica et Cosmochimica Acta*, *68*, 2081–2093.

Newell, A. J. (2005). A high-precision model of first-order reversal curve (FORC) functions for single-domain ferromagnets with uniaxial anisotropy. *Geochemistry, Geophysics, Geosystems*, *6*, Q05010. https://doi.org/10.1029/2004GC000877

Niewöhner, C., Hensen, C., Kasten, S., Zabel, M., & Schulz, H. D. (1998). Deep sulfate reduction completely mediated by anaerobic methane oxidation in sediments of the upwelling area off Namibia. *Geochimica et Cosmochimica Acta*, *62*, 455–464.

Oremland, R. S., & Taylor, B. F. (1978). Sulfate reduction and methanogenesis in marine sediments. *Geochimica et Cosmochimica Acta*, *42*, 209–214.

Ouyang, T., Heslop, D., Roberts, A. P., Tian, C., Zhu, Z., Qiu, Y., & Peng, X. (2014). Variable remanence acquisition efficiency in sediments containing biogenic and detrital magnetites: Implications for relative paleointensity signal recording. *Geochemistry, Geophysics, Geosystems*, *15*, 2780–2796. https://doi.org/10.1002/2014GC005301

Pike, C., & Fernandez, A. (1999). An investigation of magnetic reversal in submicron-scale Co dots using first order reversal curve diagrams. *Journal of Applied Physics*, *85*, 6668–6676.

Pike, C. R., Roberts, A. P., Dekkers, M. J., & Verosub, K. L. (2001). An investigation of multi-domain hysteresis mechanisms using FORC diagrams. *Physics of the Earth and Planetary Interiors*, *126*, 11–25.

Pike, C. R., Roberts, A. P., & Verosub, K. L. (1999). Characterizing interactions in fine magnetic particle systems using first order reversal curves. *Journal of Applied Physics*, *85*, 6660–6667.

Pike, C. R., Roberts, A. P., & Verosub, K. L. (2001). First-order reversal curve diagrams and thermal relaxation effects in magnetic particles. *Geophysical Journal International*, *145*, 721–730.

Pósfai, M., Buseck, P. R., Bazylinski, D. A., & Frankel, R. B. (1998a). Iron sulfides from magnetotactic bacteria: Structure, composition, and phase transitions. *American Mineralogist*, *83*, 1469–1481.

Pósfai, M., Buseck, P. R., Bazylinski, D. A., & Frankel, R. B. (1998b). Reaction sequence of iron sulfide minerals in bacteria and their use as biomarkers. *Science*, *280*, 880–883.

Reinholdsson, M., Snowball, I., Zillén, L., Lenz, C., & Conley, D. J. (2013). Magnetic enhancement of Baltic Sea sapropels by greigite magnetofossils. *Earth and Planetary Science Letters*, *366*, 137–150.

Rey, D., Mohamed, K. J., Bernabeu, A., Rubio, B., & Vilas, F. (2005). Early diagenesis of magnetic minerals in marine transitional environments: Geochemical signatures of hydrodynamic forcing. *Marine Geology*, *215*, 215–236.

Richter, C., Hayashida, A., Guyodo, Y., Valet, J. P., & Verosub, K. L. (1999). Magnetic intensity loss and core diagenesis in long-core samples from the East Cortez Basin and the San Nicolas Basin (California Borderland). *Earth, Planets and Space*, *51*, 329–336.

Riedinger, N., Formolo, M. J., Lyons, T. W., Henkel, S., Beck, A., & Kasten, S. (2014). An inorganic geochemical argument for coupled anaerobic oxidation of methane and iron reduction in marine sediments. *Geobiology*, *12*, 172–181.

Riedinger, N., Pfeifer, K., Kasten, S., Garming, L. F. L., Vogt, C., & Hensen, C. (2005). Diagenetic alteration of magnetic signals by anaerobic oxidation of methane related to a change in sedimentation rate. *Geochimica et Cosmochimica Acta*, *69*, 4117–4126.

Roberts, A. P. (1995). Magnetic characteristics of sedimentary greigite (Fe_3S_4). *Earth and Planetary Science Letters*, *134*, 227–236.

Roberts, A. P. (2015). Magnetic mineral diagenesis. *Earth-Science Reviews*, *151*, 1–47.

Roberts, A. P., Almeida, T. P., Church, N. S., Harrison, R. J., Heslop, D., Li, Y. L., et al. (2017). Resolving the origin of pseudo-single domain magnetic behavior. *Journal of Geophysical Research: Solid Earth*, *122*, 9534–9558. https://doi.org/10.1002/2017JB014860

Roberts, A. P., Chang, L., Heslop, D., Florindo, F., & Larrasoaña, J. C. (2012). Searching for single domain magnetite in the 'pseudo-single-domain' sedimentary haystack: Implications of biogenic magnetite preservation for sediment magnetism and relative paleointensity determinations. *Journal of Geophysical Research*, *117*, B08104. https://doi.org/10.1029/2012JB009412

Roberts, A. P., Chang, L., Rowan, C. J., Horng, C. S., & Florindo, F. (2011). Magnetic characteristics of sedimentary greigite (Fe_3S_4): An update. *Reviews of Geophysics*, *49*, RG1002. https://doi.org/10.1029/2010RG000336

Roberts, A. P., Florindo, F., Chang, L., Heslop, D., Jovane, L., & Larrasoaña, J. C. (2013). Magnetic properties of pelagic marine carbonates. *Earth-Science Reviews*, *127*, 111–139.

Roberts, A. P., Florindo, F., Larrasoaña, J. C., O'Regan, M. A., & Zhao, X. (2010). Complex polarity pattern at the (former) Plio-Pleistocene global stratotype section at Vrica (Italy): Remagnetization by magnetic iron sulphides. *Earth and Planetary Science Letters*, *292*, 98–111.

Roberts, A. P., Heslop, D., Zhao, X., & Pike, C. R. (2014). Understanding fine magnetic particle systems through use of first-order reversal curve diagrams. *Reviews of Geophysics*, *52*, 557–602. https://doi.org/10.1002/2014RG000462

Roberts, A. P., Jiang, W. T., Florindo, F., Horng, C. S., & Laj, C. (2005). Assessing the timing of greigite formation and the reliability of the Upper Olduvai polarity transition record from the Crostolo River, Italy. *Geophysical Research Letters*, *32*, L05307. https://doi.org/10.1029/2004GL022137

Roberts, A. P., Liu, Q. S., Rowan, C. J., Chang, L., Carvallo, C., Torrent, J., & Horng, C. S. (2006). Characterization of hematite (α-Fe_2O_3), goethite (α-FeOOH), greigite (Fe_3S_4), and pyrrhotite (Fe_7S_8) using first-order reversal curve diagrams. *Journal of Geophysical Research*, *111*, B12S35. https://doi.org/10.1029/2006JB004715

Roberts, A. P., Pike, C. R., & Verosub, K. L. (2000). First-order reversal curve diagrams: A new tool for characterizing the magnetic properties of natural samples. *Journal of Geophysical Research*, *105*, 28,461–28,475. https://doi.org/10.1029/2000JB900326

Roberts, A. P., & Turner, G. M. (1993). Diagenetic formation of ferrimagnetic iron sulphide minerals in rapidly deposited marine sediments, South Island, New Zealand. *Earth and Planetary Science Letters*, *115*, 257–273.

Roberts, A. P., & Weaver, R. (2005). Multiple mechanisms of remagnetization involving sedimentary greigite (Fe_3S_4). *Earth and Planetary Science Letters*, *231*, 263–277.

Robertson, D. J., & France, D. E. (1994). Discrimination of remanence-carrying minerals in mixtures, using isothermal remanent magnetisation acquisition curves. *Physics of the Earth and Planetary Interiors*, *84*, 223–234.

Robinson, S. G., Sahota, J. T. S., & Oldfield, F. (2000). Early diagenesis in North Atlantic abyssal plain sediments characterized by rock-magnetic and geochemical indices. *Marine Geology*, *163*, 77–107.

Rochette, P., Mathé, P. E., Esteban, L., Rakoto, H., Bouchez, J. L., Liu, Q. S., & Torrent, J. (2005). Non-saturation of the defect moment of goethite and fine-grained hematite up to 57 Teslas. *Geophysical Research Letters*, *32*, L22309. https://doi.org/10.1029/2005GL024196

Rowan, C. J., & Roberts, A. P. (2006). Magnetite dissolution, diachronous greigite formation, and secondary magnetizations from pyrite oxidation: Unravelling complex magnetizations in Neogene marine sediments from New Zealand. *Earth and Planetary Science Letters*, *241*, 119–137.

Rowan, C. J., & Roberts, A. P. (2008). Widespread remagnetizations and a new view of Neogene tectonic rotations within the Australia-Pacific plate boundary zone, New Zealand. *Journal of Geophysical Research*, *113*, B03103. https://doi.org/10.1029/2006JB004594

Rowan, C. J., Roberts, A. P., & Broadbent, T. (2009). Reductive diagenesis, magnetite dissolution, greigite growth and paleomagnetic smoothing in marine sediments: A new view. *Earth and Planetary Science Letters*, *277*, 223–235.

Rudmin, M., Roberts, A. P., Horng, C. S., Mazurov, A., Savinova, O., Ruban, A., et al. (2018). Ferrimagnetic iron sulfide formation and methane venting across the Paleocene-Eocene Thermal Maximum in shallow marine sediments, ancient West Siberian Sea. *Geochemistry, Geophysics, Geosystems*, *19*, 21–42. https://doi.org/10.1002/2017GC007208

Segarra, K. E. A., Comerford, C., Slaughter, J., & Joye, S. B. (2013). Impact of electron acceptor availability on the anaerobic oxidation of methane in coastal freshwater and brackish wetland sediments. *Geochimica et Cosmochimica Acta*, *115*, 15–30.

Shi, M. N., Wu, H. C., Roberts, A. P., Zhang, S. H., Zhao, X. X., Li, H. Y., et al. (2017). Tectonic, climatic, and diagenetic control of magnetic properties of sediments from Kumano Basin, Nankai margin, southwestern Japan. *Marine Geology*, *391*, 1–12.

Sivan, O., Adler, M., Pearson, A., Gelman, F., Bar-Or, I., & John, S. G. (2011). Geochemical evidence for iron-mediated anaerobic oxidation of methane. *Limnology and Oceanography*, *56*, 1536–1544.

Tric, E., Laj, C., Jehanno, C., Valet, J. P., Kissel, C., Mazaud, A., & Iaccarino, S. (1991). High-resolution record of the Upper Olduvai transition from Po Valley (Italy) sediments: Support for dipolar transition geometry? *Physics of the Earth and Planetary Interiors*, *65*, 319–336.

van Dongen, B. E., Roberts, A. P., Schouten, S., Jiang, W. T., Florindo, F., & Pancost, R. D. (2007). Formation of iron sulfide nodules during anaerobic oxidation of methane. *Geochimica et Cosmochimica Acta*, *71*, 5155–5167.

Vasiliev, I., Dekkers, M. J., Krijgsman, W., Franke, C., Langereis, C. G., & Mullender, T. A. T. (2007). Early diagenetic greigite as a recorder of the palaeomagnetic signal in Miocene-Pliocene sedimentary rocks of the Carpathian foredeep (Romania). *Geophysical Journal International*, *171*, 613–629.

Weaver, R., Roberts, A. P., & Barker, A. J. (2002). A late diagenetic (syn-folding) magnetization carried by pyrrhotite: Implications for paleomagnetic studies from magnetic iron sulphide-bearing sediments. *Earth and Planetary Science Letters*, *200*, 371–386.

Wehland, F., Stancu, A., Rochette, P., Dekkers, M. J., & Appel, E. (2005). Experimental evaluation of magnetic interaction in pyrrhotite bearing samples. *Physics of the Earth and Planetary Interiors*, *153*, 181–190.

Yamazaki, T. (2008). Magnetostatic interactions in deep-sea sediments inferred from first-order reversal curve diagrams: Implications for relative paleointensity normalization. *Geochemistry, Geophysics, Geosystems*, *9*, Q02005. https://doi.org/10.1029/2007GC001797

Yamazaki, T. (2009). Environmental magnetism of Pleistocene sediments in the North Pacific and Ontong-Java Plateau: Temporal variations of detrital and biogenic components. *Geochemistry, Geophysics, Geosystems*, *10*, Q07Z04. https://doi.org/10.1029/2009GC002413

Yamazaki, T., Abdeldayem, A. L., & Ikehara, K. (2003). Rock-magnetic changes with reduction diagenesis in Japan Sea sediments and preservation of geomagnetic secular variation in inclination during the last 30,000 years. *Earth, Planets and Space*, *55*, 327–340.

Yamazaki, T., & Ikehara, M. (2012). Origin of magnetic mineral concentration variation in the Southern Ocean. *Paleoceanography*, *27*, PA2206. https://doi.org/10.1029/2011PA002271

Zhao, X., Roberts, A. P., Heslop, D., Paterson, G. A., Li, Y. L., & Li, J. H. (2017). Magnetic domain state diagnosis using hysteresis reversal curves. *Journal of Geophysical Research: Solid Earth*, *122*, 4767–4789. https://doi.org/10.1002/2016jb013683